

THE MICRORHEOLOGY OF LIPID BILAYERS

by

TRISTAN HORMEL

A DISSERTATION

Presented to the Department of Physics
and the Graduate School of the University of Oregon
in partial fulfillment of the requirements
for the degree of
Doctor of Philosophy

June 2015

DISSERTATION APPROVAL PAGE

Student: Tristan Hormel

Title: The Microrheology of Lipid Bilayers

This dissertation has been accepted and approved in partial fulfillment of the requirements for the Doctor of Philosophy degree in the Department of Physics by:

John Toner	Chair
Raghuveer Parthasarathy	Advisor
Eric Corwin	Core Member
Kelly Sutherland	Institutional Representative

and

Scott L. Pratt	Dean of the Graduate School
----------------	-----------------------------

Original approval signatures are on file with the University of Oregon Graduate School.

Degree awarded June 2015

© 2015 Tristan Hormel

This work is licensed under a Creative Commons
Attribution-NonCommercial-NoDerivs (United States) License.

DISSERTATION ABSTRACT

Tristan Hormel

Doctor of Philosophy

Department of Physics

June 2015

Title: The Microrheology of Lipid Bilayers

Microrheology has successfully illuminated and quantified the material properties of small, three dimensional fluid samples. It has been less often utilized to examine the two dimensional viscosity of materials such as the lipid bilayer, where several complications make experiments difficult. Here, I discuss two new methods that should provide a general framework for characterizing the fluid properties of two dimensional materials.

This dissertation includes previously published and unpublished coauthored material.

CURRICULUM VITAE

NAME OF AUTHOR: Tristan Hormel

GRADUATE AND UNDERGRADUATE SCHOOLS ATTENDED:

University of Oregon, Eugene, OR
Reed College, Portland, OR

DEGREES AWARDED:

Doctor of Philosophy, Physics, 2015, University of Oregon
Bachelor of Arts, Physics, 2009, Reed College

AREAS OF SPECIAL INTEREST:

Rheology of lipid bilayers

PROFESSIONAL EXPERIENCE:

Research Assistant, Parthasarathy Group

GRANTS, AWARDS AND HONORS:

NSF GK-12 Fellow, Scientist in Residence, University of Oregon, 2015

PUBLICATIONS:

T. Hormel, S. Kurihara, M. Brennan, M. Wozniak and R. Parthasarathy. Measuring lipid membrane viscosity using rotational and translational probe diffusion. *Physical Review Letters*, 112:188101, 2014.

ACKNOWLEDGEMENTS

Several undergraduates helped with experiments and deserve thanks: Morgan Hynson, Katie Brennan, Matthew Wozniak, and especially Sarah Kurihara and Matthew Reyer. Labmates also helped with experiments, even if they didn't conduct them: Ryan Baker, Matthew Jemelieta, Andrew Loftus and Mike Taormina all provided valuable discussions and insight. For non-academic support, friends and family and in particular Marial Torres my cats Cheepie Caloo and Barnaby Jones. The National Science Foundation funded my research. My advisor Raghu Parthasarathy, from whom I have learned so much about being a scientist, deserves special thanks. Finally, support from NSF Awards 1006171 and 0742540 funded this work.

For my parents.

TABLE OF CONTENTS

Chapter	Page
I. INTRODUCTION	1
The Cell Membrane	1
II. MOLECULES, MEMBRANES AND MODELS	4
Membrane Biochemistry	4
Membrane Fluid Mechanics	12
Conclusion	18
III. MEASUREMENTS AND MICRORHEOLOGY	19
Image Processing	20
Diffusion Measurements	24
Parameter Estimation	25
Conclusion	27
IV. EXPERIMENTS AND RESULTS	28
Introduction	28
Rotating Tracers	28
Two-point Microrheology	38
V. CONCLUSION AND OUTLOOK	49
REFERENCES CITED	53

LIST OF FIGURES

Figure	Page
1. Space filling models of lipids	6
2. Bond line models of lipids	6
3. Bond and space filling models of cholesterol	8
4. Bilayer phases	10
5. Stokes drag	14
6. Simulated localization error of elliptical tracers	23
7. Rotating tracer experimental setup	31
8. Diffusive behavior of rotating tracers	32
9. Effective inclusion radius and viscosity of a DOPC bilayer	35
10. Membrane viscosity modulated by Sar1	36
11. Fluorescence images of giant unilamellar vesicles	41
12. Diffusion of phase separated domains	43
13. One-point viscosity of phase separated giant unilamellar vesicles	44
14. Two-point viscosity of phase separated giant unilamellar vesicles	45
15. One- and two-point viscosity of different bilayer compositions	47
16. Effect of tension on bilayer viscosity	51

LIST OF TABLES

Table	Page
1. Lipid composition of a cell	7

CHAPTER I

INTRODUCTION

If you can read this, you are doing so with biological machinery selected through a four billion year history of evolution. Your eyes, that can see the words, and your brain, than can understand them, are products of this rich history, as is every organ used to construct a creature capable of reading. As is a human being in its entirety, and every other living thing on Earth. This history is a story as much of accident as much innovation. Its result are the millions of species alive today.

To understand this staggering diversity in all of its complexity is the unenviable task of the biologist. As a biophysicist, I'm tempted to seek unifying principles analogous to Newton's gravity, that explains both falling apples and orbiting planets. But from a superficial inspection, this seems nothing short of hopeless. That there are unifying principles that can describe a whale as well as a flea seems unlikely. But nonetheless, that such unifying principles do in fact exist is obvious inasmuch as we can learn about ourselves by studying *Eschericia coli*. Some such unifying principles are conceptual- there is a logic to evolution, and biology is as subject to physics as is chemistry. But others are concrete and material- all living things make use of DNA, of the same amino acids.

My dissertation research is an attempt to develop tools that will help us understand another such universal feature of cellular life: the lipid bilayer. This structure is the foundational, essential component of all biological membranes, and by any assessment one of the most important structures in biology.

The Cell Membrane

While the lipid bilayer is the essential component of a cell membrane, you might not know it by looking at one. In fact even in the middle of the twentieth century there was debate a to whether lipids or proteins constituted the essential component of a living membrane[2]. This isn't really an odd confusion. Cell membranes often contain an appreciable amount of proteins by weight, sometimes even exceeding the lipid content[3]. The variety of these proteins is a testament to the importance of the membrane structure to life: in *E. Coli*, which has the most understood

genome, almost a quarter of genes code for membrane proteins[4]. There are many reasons for this variety, a corollary to the many roles that cell membranes play in cellular function. As the barrier that separates a cell's interior from its exterior, any interaction with a cell's environment must be mediated through the membrane. It also serves as a semi-permeable barrier, keeping biological molecules and cellular contents localized to different regions where they can be useful to the cell. Flexibility, or deformability, is another key requirement, in part because cells will sometimes wish to ingest large amounts of material, for instance through phagocytosis, but especially because major requirement for all life on a cellular scale is division. All of these functions require families of proteins and other macromolecules. The physical mechanisms that govern the organization of these proteins on the cell's surface is an area of research rife with controversy, particularly with respect to lipid rafts[5]- the point being that now is a good time to study membranes.

The fluid mosaic model of Singer and Nicholson established a view of membranes according to which the bilayer serves as a matrix on which proteins are able to move and spatially organize[6]. Singer and Nicholson emphasized the *fluidity* of the bilayer, a feature responsible for the membrane's ability to dynamically and chemically reorganize in response to a cell's needs.

Additionally, the magnitude of fluid properties of the bilayer, such as bilayer viscosity, are in their own right biological parameters of important scope. The timescale for diffusion in a membrane is set by bilayer viscosity, and therefore viscosity sets a physical limit on the speed with which cells can perform certain functions. At a different lengthscale, viscosity also determines how much a membrane will deform in response to an in-plane force, and so will also be a determining feature for how quickly cells can stretch and broadly change their shape.

If, then, we wish to model any such cellular process, we will require good measurements of membrane viscosity. My dissertation research is an attempt to make such measurements, but also to develop improved methodologies for making them. The hope is that, in the future, we will have the means to make relatively easy and precise measures of the viscosity of two-dimensional fluids.

This document is divided in to five chapters. In the second, I discuss some of the chemistry and fluid mechanics that inform our understanding of lipid bilayers. This includes the chemical nature of the lipids that form bilayers, and how that chemistry informs bilayer viscosity. I also discuss continuum models of diffusion in membranes; these models have been broadly, but not universally, successful in describing the motion of inclusions within membranes.

In the third chapter, I discuss the analytical and computational tools needed to perform a microrheology experiment like those I performed. These are specific cases of problems, such as feature localization, within the larger field of image analysis. The information in this chapter is summary and general.

The fourth chapter contains the experimental details and results of my experiments. These are the main conclusions of my dissertation research. The specifics of analytic and experimental approaches we used for each project will be found here. This chapter includes material coauthored with Sarah Kurihara, Kathleen Brennan, Matthew Wozniak, Matthew Reyer and Raghuveer Parthasarathy.

The final chapter offers concluding remarks and some ideas for extensions of my work that could be performed by another researcher.

CHAPTER II

MOLECULES, MEMBRANES AND MODELS

Even though the cell membrane is a small structure, there are a lot of ways to characterize it. In this chapter, I'll present details of two such characterizations, one which relies on the physical chemistry of the bilayer and another which considers the fluid mechanics of two-dimensional membranous structures. Throughout, the membranes I'll discuss will be simplified, cell-free lipid bilayers, devoid of the proteins and other cellular machinery that complicate the real things in real life.

Membrane Biochemistry

The experiments I performed are amenable to continuum descriptions of lipid bilayers. That is, given the size of relevant experimental features, we were able to ignore the molecular nature of the bilayer in our calculations and measurements. Nonetheless a few words on the constituents of these membranes, lipids and otherwise, are in order. In particular, lipid structural properties can illuminate some of the characteristics of the bilayers that they form, including bilayer viscosity.

Lipid Species

Lipids are an enormous class of molecules, and approximately 5% of genes are used in synthesizing many different types[7]. Taken in the broadest sense, they comprise not just the bilayer forming lipids present in cell membranes, but also a host of other compounds with varying degrees of complexity and size[8]. The latter include detergents (such as sodium dodecylsulfate, familiar to shampoo users) and some vitamins, while an important example of the former are the phospholipids.

All lipids are amphipathic molecules, composed of a hydrophilic (water-loving) region, and a hydrophobic (water-hating) region. In phospholipids the hydrophobic region is termed a "headgroup", while the hydrophobic region is composed of hydrocarbon (acyl) chains of varying length (Fig. 1 and 2). The core, or conserved, portion of phospholipids is a glycerol molecule, or

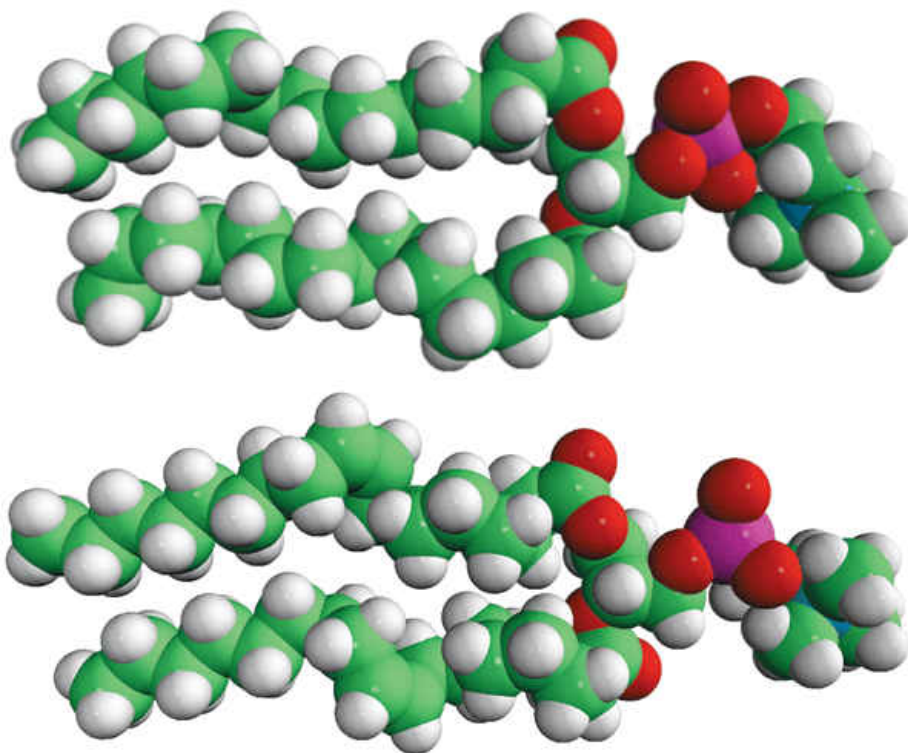
backbone, attached to a phosphomoiety[8] containing headgroup (Fig. 1 and 2).¹. Many different headgroups are used by cells, and the headgroup is one feature that distinguishes different categories of phospholipids. Phosphatidylcholines, or PC lipids, comprise one of the most studied and most common groups, and are the subject of my research, but phosphatidylethanolamines (PE) and phosphatidylserines (PS) are also abundant and well-studied. The glycerol core is also bound to two acyl chains. The length and saturation of these chains is another distinguishing feature of phospholipids². While phospholipids differentiated by acyl chain structure always carry different chemical names, due to the large number of phospholipid varieties these names can be clunky; and it is therefore often easier and more illuminating, especially when considering lipids with a common headgroup, to refer to lipids by (chain length):(number of double bonds). For instance, 1,2-dioleoyl-sn-glycero-3-phosphocholine, DOPC, and 18:1 PC all refer to the same molecule (Fig. 2(b)), as do 1,2-dipalmitoyl-sn-glycero-3-phosphocholine, DPPC and 16:0 PC, respectively (Fig 2(c)), but the 18:1 PC and 16:0 PC nomenclature make the differences between the two most obvious, at least for a physicist. When one is interested in discussing the location of a particular bond in the acyl chain, this is done by referring to a Δ position, which is the number of carbon bonds from the headgroup. So, for example, DOPC has a double bond at the Δ 9 position. Furthermore, the conformation of the tail chains is important in lipid phase behavior. Carbon bonds in lipid acyl chains have two conformations, either *cis* or *trans*³ (Fig 2). The *cis* conformation places a bend in the acyl chain that increases the cross-sectional area of the lipid molecule[9]. Unsaturated double bonds are almost always found in the *cis* conformation, while single bonds can be found in either, dependent upon bilayer phase[10] (see section 2.1.2).

Phospholipids are not the only lipids found in biological membranes. Table 1 gives the lipid composition of several membranes from several lifeforms. Like phospholipids, sphingolipids are complex lipids with a polar headgroup and acyl chains. Some biological membranes also contain cholesterol (Fig 3). Cholesterol is a sterol lipid that, on its own, does not form bilayers. It is, however, readily incorporated into phospholipid and especially sphingolipid bilayers[11]. It is present in large quantities in the plasma membrane of eukaryotes, where it can be present at

¹Phospholipids are also termed glycerophospholipids, but in practice they are almost always referred to using the briefer designation.

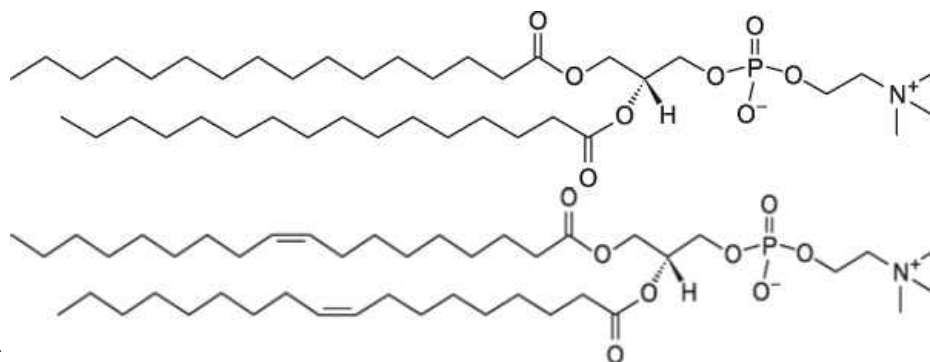
²In saturated chains, every carbon atom in the chain is bound to other carbons with just single bonds, while the other bonds are filled with hydrogen; unsaturated chains contain one or more double bonds between carbon atoms.

³These terms come from the latin *cis* = this side, *trans* = the other side.



filling.png

FIGURE 1. Space filling models for DPPC (top) and DOPC (bottom). Tail bonds are in the trans conformation, with the exception of the cis double bond at the $\Delta 9$ position in DOPC. Images from Avanti Polar Lipids.



line.png

FIGURE 2. Bond line models for the same lipids, DPPC (top) and DOPC (bottom). Images from Avanti Polar Lipids.

Compartment	Plasmamembrane	Endoplasmic Reticulum	Golgi	Lysosome	Nuclear Membrane
lipid					
phosphatidylcholine	18	48	25	23	44
phosphatidylethanolamine	12	19	9	13	17
phosphatidylserine	7	4	3	0	4
phosphatidylinositol	3	8	5	6	6
sphingomyelin	12	5	7	23	3
cardiolipin	0	0	0	0	5
glycolipid	8	traces	0	0	traces
others	21	10	43	16	15
cholesterol	19	6	8	14	10

TABLE 1. Lipid components of membranes in rat liver cells. Taken from ref. [1]

molar concentrations of up to 45%[12]. The enzymatic pathway that produces cholesterol is long and energy intensive, requiring over three dozen steps, including 18 steps to obtain cholesterol from a similar sterol, lanosterol[8]. In mammalian cell membranes, cholesterol seems to serve a number of purposes, including direct modulation of the activity of some proteins[13, 14]. Cholesterol also has a profound effect on membrane fluidity, and especially the phase behavior, of lipid bilayers.

Lipid Phases

Because they are amphipathic, lipids in aqueous environments will form structures that simultaneously shelter hydrophobic regions from and expose hydrophilic regions to the surrounding solvent. The bilayer, oriented such that the acyl chains are sandwiched between two layers of polar headgroups, obviously has this property. But the bilayer is only one of several structures lipids form in aqueous solution[15]. Additionally, the bilayer itself is not organized in just a single way- there are in fact several bilayer phases. Collectively, these are termed lamellar phases, while any non-bilayer phase is nonlamellar⁴. What phases can form depend on the chemical identity of the lipid— even within bilayer forming lipids, like phospholipids, there is variation[16]. DPPC, for example, can form any lamellar phase, but some phospholipids with short chains in particular will not form some bilayer phases and will instead create micelles, a nonlamellar phase in which lipids pack into spheres with hydrophobic acyl chains pointing inward.

⁴Another distinction often encountered is between unilamellar, as in giant unilamellar vesicle, and multilamellar phases. Multilamellar phases are usually considered nonlamellar.

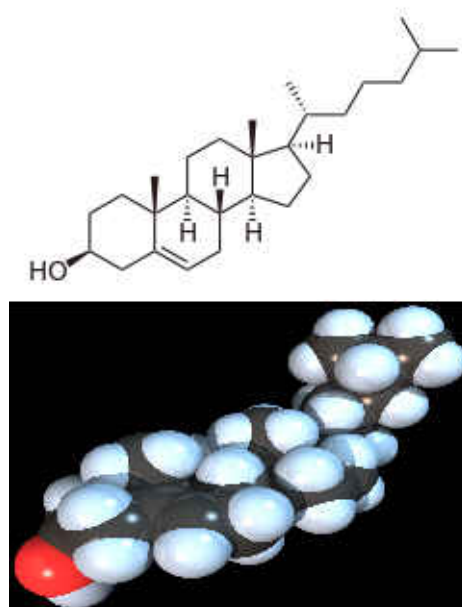


FIGURE 3. Bond line (top) and space filling (bottom) models of cholesterol. Images from wikipedia.

In general, both acyl chain length and polar headgroup size are important determinants of lipid phase behavior[17]. However, headgroup interactions are hard to modify[1], while lipids with different chain lengths are readily available. This means that in practice, it is often easier to study the effect of chain length and conformation on bilayer properties, an approach that we adopted in our experiments.

Bilayers transition between different lamellar phases due to changes in temperature, pressure, composition, tension and hydration. Of these, temperature is especially convenient to examine experimentally. Differential Scanning Calorimetry (DCM) can be used to determine the temperature of different bilayer phase transitions when other variables are held constant[18]; DCM studies can be combined with Nuclear Magnetic Resonance (NMR) or Fourier Transform Infrared spectroscopy (FTIR) to determine the conformation of the bilayer in the different phases[19].

The simplest lamellar phase behavior is seen in bilayers containing just a single component. Such systems are therefore important models for investigating lipid phase behavior. Single component membranes exhibit one fluid, or liquid crystalline, and several sub-fluid gel and

crystalline phases. Bilayers formed from DPPC, the most studied single component system⁵, will form all four phases[8].

In all of the gel and crystalline phases, saturated acyl chains are fully extended (i.e., the hydrocarbon chains contain only trans conformers; see Fig. 4). The lowest temperature state is the pseudocrystalline L_C phase. Here lipid motion is severely restricted. Lipids pack in a formation that is similar to their crystalline dehydrate. With increasing temperature, the bilayer enters the gel phase. This state has several polymorphisms, in each of which lipids slowly rotate. One of the polymorphisms, confusingly, is termed the gel phase L_β . Here, the lipids pack in to orthorhombic lattice. In the tilted gel phase, $P_{\beta'}$, lipids tilt with respect to the bilayer normal. As temperature is increased further, the bilayer will enter the Ripple P_β phase. Here, the lipids exhibit faster rotation and are packed in a hexagonal lattice. Lipids are displaced vertically, so that the bilayer no longer exists in a plane, but is rippled.[8]

The main transition, called the chain melting transition, occurs when the highly ordered acyl chains of the gel phases melt; this creates the fluid L_α phase, also called the liquid crystalline or liquid disordered (L_D) phase. In contrast to gel phases, where acyl chains are extended, in the L_D phase chains have both cis and trans bonds. For DPPC, with its 16 carbon chains, on average 3.9 bonds will be in the cis configuration[10]. The bonds most often form “kinks” by adopting a cis-trans-cis configuration[20]. These kinks, and the cis bond angles in general, have the effect of frustrating the hexagonal packing of the gel phases. As a result, lipids occupy a greater area, and are more free to rotate. All of this has the result of markedly increasing the fluidity of the membrane: the translational diffusion coefficient for lipids in a liquid crystalline bilayer is $\approx 1 \mu\text{m}^2/\text{s}$ [21], orders of magnitude faster than the equivalent value in a gel phase bilayer ($\approx 1 \times 10^{-2}$ - $1 \times 10^{-3} \mu\text{m}^2/\text{s}$)[22, 23].

Understanding the phase behavior of a single component bilayer will obviously be an important step in attaining a similar understanding for living membranes. Nonetheless, it is worth emphasizing that if a single component phospholipid bilayer membrane is to serve as a model of a biological membrane, it is an extremely reductionist one. At the very least, living membranes are replete with sometimes hundreds of different varieties of proteins[4] (which, in total, can outweigh the lipid components of living membranes[3]), and carbohydrates. Any of these might

⁵DPPC is particularly well studied primarily for two reasons: (1) it readily forms bilayers, and so is easy to work with, and (2) it is of a headgroup type and chain length that are widely utilized in living cells.

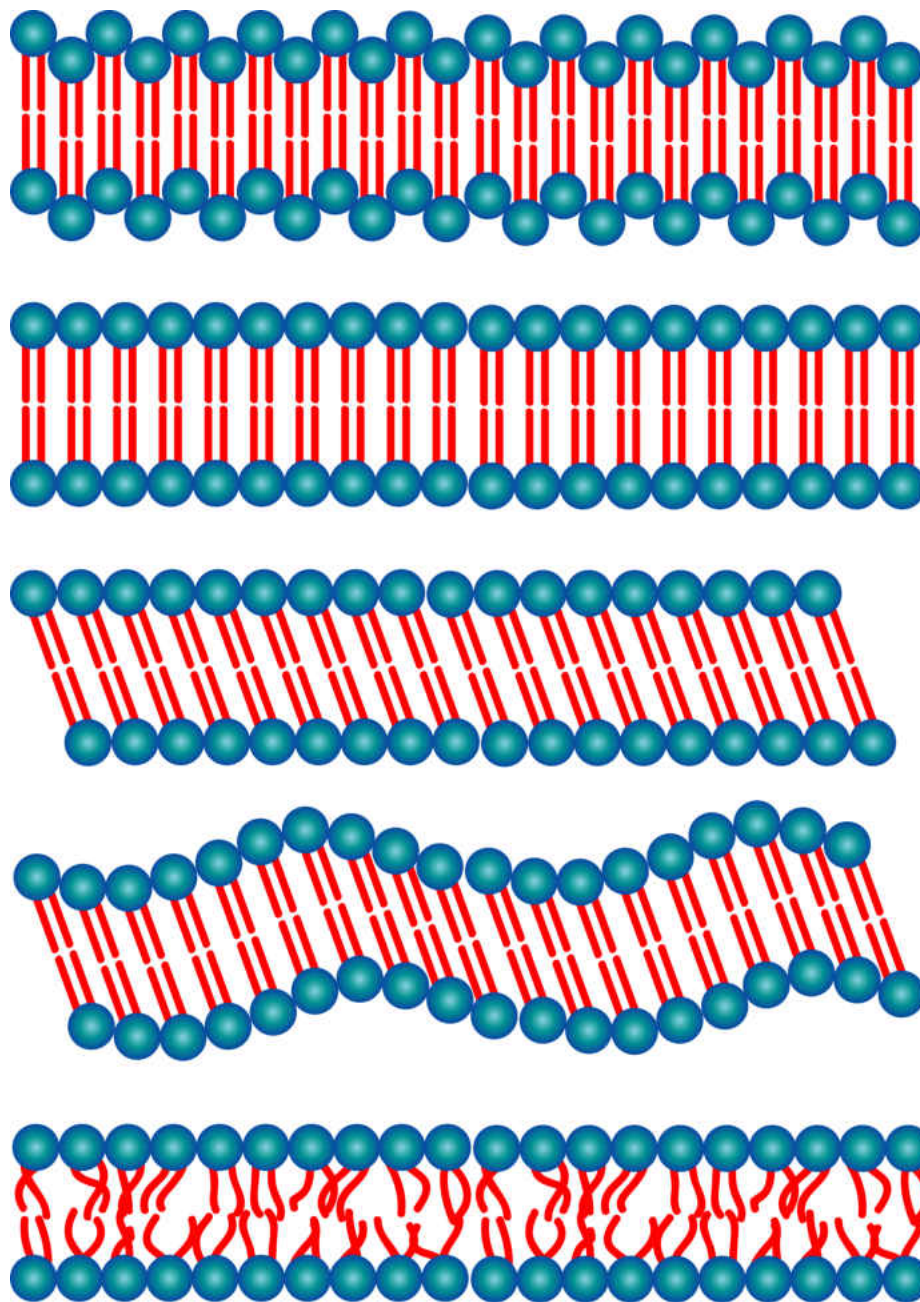


FIGURE 4. Schematic. Different bilayer phases, top to bottom: Pseudocrystalline, gel, tilted gel, ripple gel, and liquid disordered.

reasonably be expected to significantly affect the phase behavior of the constituent lipid bilayer. Furthermore, cells employ not just a single species of lipid when building their membranes, but thousands[24]. It is therefore also important that we understand the phase behavior of lipid mixtures. In particular, two obvious questions are (1) do multicomponent bilayers form the same phases as single component membranes; and (2) how are different lipid species distributed in the bilayer?

These questions are actually related: multicomponent bilayers can, in the right conditions, phase separate into domains rich in a certain lipid species and depleted of another, creating heterogeneous bilayers with gel and fluid regions. An important case of this behavior is cholesterol-mediated, and involves a cholesterol dependent phase. This phase, termed liquid ordered (L_O), is in many ways intermediate between gel phases and the liquid disordered state. It occurs at temperatures below the chain melting temperature (although it should be noted that cholesterol affects this temperature in the phospholipids in complex ways that depend on both headgroup structure and acyl chain length[17, 25]), and so acyl chains are extended. On the other hand lateral lipid diffusion more closely resembles the L_D phase, though it is still slowed ($6.9 \mu\text{m}^2/\text{s}$ in the L_D phase[21] vs. $3.3 \mu\text{m}^2/\text{s}$ in L_O phase[26] for DMPC at 43°C , for example). Cholesterol also affects acyl chain order and lipid packing above the melting transition temperature; lipid tails appear more ordered in the presence of cholesterol[27]. Finally, even when phospholipids will phase separate in the presence of cholesterol, the literature is somewhat unclear with respect to the location of cholesterol itself. There is broad agreement that living membranes contain L_O domains rich in cholesterol[28], but at least in two PC component bilayers with cholesterol the cholesterol doesn't seem to have a preference for L_O or L_D domains[22].

Multicomponent, phase separated bilayers are an especially important model systems for experimentalists. They have an instructive appeal, as they represent a midway point between gross complexity of cell membranes, from which it is difficult to draw organizing principles, and single-component or homogeneous bilayers, from which biological inference is questionable. More importantly, they possess an immense experimental utility. Fluorescently labeled lipids can themselves partition in to a particular lipid phase, and when included in small quantities in model membranes they provide a convenient means through which phase separation can be viewed[29]. A number of experiments utilize these visibly phase separated domains[30–33]. Particularly relevant

is that, since the domains undergo Brownian diffusion, they can be used to measure membrane viscosity[34, 35]; see chapter 4.

Membrane Fluid Mechanics

Now I will take a larger view, and consider the bilayer on a scale at which the motions and conformations of individual molecules are smeared out. That is, I want to investigate a description of bilayer fluidity that relies not on the organization of lipid molecules, but instead is parametrized by fluid properties such as viscosity. I will focus mostly on diffusion of objects embedded in membranes. There are two reasons that diffusion is an especially important in this context: (1) living organisms make extensive use of diffusion, and so the phenomenon is of intrinsic biological interest, and (2) measurements of diffusion can be used determine bilayer fluid properties. This second point is the motivation for microrheological experiments, and the logic is the reason that we are able to engage in such measurements in the first place.

Einstein Relations

We begin by considering a suspension of particles of mass m in a homogeneous fluid⁶. The system is in equilibrium, and acted on by a gravitational force in the z direction $F_z = mg$. We'll begin by writing the continuity equation

$$\frac{\partial \rho}{\partial t} + \nabla \cdot \mathbf{j} = 0, \quad (2.1)$$

where $\rho(\mathbf{r}, t)$ is the particle density at \mathbf{r} at time t , and $\mathbf{j}(\mathbf{r}, t)$ is the particle flux. In a steady state, $\frac{\partial \rho}{\partial t} = 0$, so we only need concern ourselves with the particle flux. This term can be broken into parts: a deterministic portion due to particle sedimentation, and a stochastic portion due to Brownian motion. To obtain the former, we can balance forces to get the sedimentation speed

$$\mathbf{v}(\mathbf{r}, t) = -\frac{mg}{b} \hat{z}, \quad (2.2)$$

⁶This derivation follows my notes from one of John Toner's classes.

where b is the drag on the particles. We'll calculate the drag on particles in membranes in the next section, but for now we can treat it as a constant⁷. Then the deterministic flux is just

$$\mathbf{j}_{\text{Det}} = -\rho \frac{mg}{b} \hat{z}. \quad (2.3)$$

Meanwhile, Fick's Law gives contribution to flux from diffusion:

$$\mathbf{j}_{\text{Sto}} = -D\nabla\rho. \quad (2.4)$$

Combining, the continuity equation (2.1) becomes

$$-\frac{mg}{b} \frac{\partial\rho}{\partial z} - D\nabla^2\rho = 0. \quad (2.5)$$

The only interesting direction is \hat{z} :

$$\frac{d^2\rho}{dz^2} = -\frac{mg}{bD} \frac{d\rho}{dz}, \quad (2.6)$$

which can be solved by

$$\rho(z) = \rho_0 e^{-\frac{mgz}{bD}}, \quad (2.7)$$

where I've chosen boundary conditions such that $\rho(z \rightarrow \infty) = 0$. This molecular view must match Boltzmann's answer

$$\rho(z) = \rho_0 e^{-\frac{mgz}{k_B T}}, \quad (2.8)$$

which requires

$$D = \frac{k_B T}{b}. \quad (2.9)$$

Einstein Relation

⁷In principle, the drag b will depend on properties of the fluid and the suspended particles, but for this derivation none of these quantities will vary.

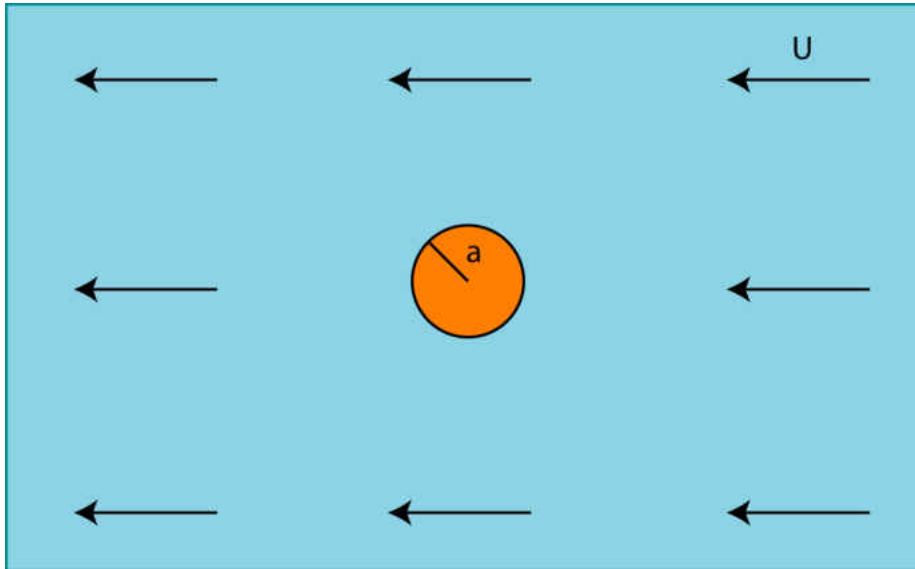


FIGURE 5. Setup for calculating the Stokes drag on a circle embedded in a 2D fluid. The fluid moves with velocity U far from the inclusion. At the edge of the inclusion, the fluid is stationary.

(2.9) is called the Einstein relation. The essential feature that makes (2.9) so useful is that it provides a connection between fluctuations (of which Brownian motion is an example) and energy dissipation (drag). In this respect it is just one of several instances of the fluctuation-dissipation theorem, a subject that has received considerable theoretical attention[36]. Experimentally, it suggests a method of relating an observable phenomenon (the random motion of a particle) to underlying features of the material in which it is embedded. This connection forms the basis of passive microrheological techniques. However, if we are to use (2.9) to measure fluid properties, we still must connect the drag to these fluid properties. In principle, this is simple, and the drag on a sphere in three dimensions, for instance, takes a satisfyingly simple form. For an object embedded in a two-dimensional membrane, however, the calculation is problematic.

The Stokes Paradox

The drag we wish to calculate is the translational drag⁸ on a cylinder of radius a embedded in a two dimensional surface, as shown in Fig 5.

⁸A similar derivation for the rotational drag on a cylinder in a 2D membrane does not encounter the difficulties that will become evident below.

The incompressible fluid in which the cylinder is embedded moves with velocity \mathbf{u} in one direction at a steady rate. To find the drag, we can begin with the equations of motion for the system, which are given by the Navier-Stokes equations for an incompressible fluid:

$$\frac{\partial \mathbf{u}}{\partial t} + \mathbf{u} \cdot \nabla \mathbf{u} - \frac{\eta}{\rho} \nabla^2 \mathbf{u} = -\frac{1}{\rho} \nabla p + \mathbf{g}, \quad (2.10)$$

$$\nabla \cdot \mathbf{u} = 0 \quad \text{Navier-Stokes Equations}$$

where ρ is the fluid density, η is the fluid viscosity, and \mathbf{g} is any body accelerations acting on the fluid (for instance from gravity). (2.10) is notoriously difficult to work with in this general form, but we can get considerable mileage by making simplifications appropriate to the problem at hand. Specifically, we won't consider forces acting on the fluid, so we can ignore the final term in (2.10).

A less trivial simplification involves rewriting (2.10) in a dimensionless form. The motivation for such an action is that we can sometimes construct dimensionless quantities that are small out of the lengthscales inherent to the problem. For instance, the Reynolds number

$$Re = \frac{\rho v L}{\eta}, \quad (2.11)$$

Reynolds Number

where L is a characteristic length, represents the ratio of inertial to viscous forces. For cells and their associated machinery, Re is always small⁹. So if we are trying to derive drag on a cylinder in an cell membrane from (2.10), we can gain some traction by defining dimensionless versions of the variables appropriate to the given scales:

$$\mathbf{r}^* = \frac{\mathbf{r}}{L}, \quad \mathbf{u}^* = \frac{\mathbf{u}}{v},$$

$$t^* = \frac{t}{L/v}, \quad p^* = \frac{pL}{\eta v}.$$

⁹It almost goes without saying that, since we are talking about biology, there are exceptions to this "universal" rule.

In terms of these variables, it is possible to write (2.10) as

$$Re \left(\frac{\partial \mathbf{u}^*}{\partial t^*} + \mathbf{u}^* \cdot \nabla \mathbf{u}^* \right) = -\nabla p^* + \nabla^2 \mathbf{u}^*, \quad (2.12)$$

which indicates that for small Reynolds number we can ignore the LHS of (2.12). Returning to dimensional units, we then have

$$\nabla p = \eta \nabla^2 \mathbf{u}. \quad (2.13)$$

We can take the curl of (2.13) to eliminate ∇p . Meanwhile, since $\nabla \cdot \mathbf{u} = 0$, we can there exists ψ such that $\nabla \times \psi = \mathbf{u}$. Therefore, after taking the curl of (2.13) and performing some vector calculus and algebra, we have

$$\nabla^4 \psi = 0, \quad (2.14)$$

where ∇^4 is the biharmonic operator. Working in cylindrical coordinates, we can now separate the coordinates by taking $\psi = \sin \theta f(r)$, giving

$$\left(\frac{d^2}{dr^2} + \frac{1}{r} \frac{d}{dr} - \frac{1}{r^2} \right)^2 f = 0. \quad (2.15)$$

The general solution to (2.15) is

$$f(r) = Ar^3 + Br \log r + Cr + D \frac{1}{r}, \quad (2.16)$$

which is to be solved subject to the boundary conditions (1) $\psi(a) = \left. \frac{\partial f}{\partial r} \right|_{r=a} = 0$ (no slip boundaries), and (2) $f(r \rightarrow \infty) \propto vr$ (free flow far from the inclusion). (2) requires $A = B = 0$, and if we subsequently try to solve for C and D subject to (1), we find that we also require $C = D = 0$: (2.16) cannot be solved subject to the desired boundary conditions.

This result is Stokes' paradox. It is only a paradox in a limited sense, in that it's not too difficult to ascertain where the difficulty lies: (2.16) was derived by neglecting terms proportional to the Reynolds number; apparently these terms must contribute to the flow fields we were trying to calculate. A more strenuous calculation than the one I outlined above, obtained by keeping the

$\mathbf{u} \cdot \nabla \mathbf{u}$ term from (2.12), was obtained by Horace Lamb[37]. His result gives

$$b_T = \frac{1}{4\pi\eta} \left(\log \frac{4\eta}{\rho U a} + \frac{1}{2} - \gamma \right), \quad (2.17)$$

where γ is Euler’s constant. The problem with (2.17), however, is that the drag is now *force dependent*, which means that the argument leading to the Einstein relation (2.9) fails[38].

Membrane Fluid Mechanics

Another, real world objection to the discussion given above might be the strict restriction of the discussion to two dimensions. In 1975, Saffman and Delbrück suggested[38] that (2.9) could be salvaged by coupling flow in the two-dimensional fluid sheet with flow in a surrounding medium. Their motivation was biological: lipid bilayers are surrounded by water. By including dissipation into the surrounding bulk fluid, they calculated the drag to be

$$b_T = \frac{1}{4\pi\eta} \left(\log \frac{\eta}{\eta_w a} - \gamma \right), \quad (2.18)$$

Saffman-Delbrück Model

where η_w is the viscosity of the surrounding fluid. The expression for rotational drag calculated under identical circumstances is

$$b_R = \frac{1}{4\pi\eta a^2}. \quad (2.19)$$

Equations (2.18) and (2.19) represent the Saffman-Delbrück (SD) model. While simple, it holds only for $\epsilon = \frac{2\eta_w a}{\eta} \ll 1$; that is, for relatively small inclusions in relatively viscous membranes. If we wish to find a more general solution, we must return to (2.10) and work through the calculation explicitly for the “actual” situation: a cylindrical inclusion in a thin membrane spanning a three-dimensional bulk fluid. The mathematics quickly becomes grim, but a full analytic solution was obtained by Hughes, Pailthorpe and White (HPW) in 1981[39]. While their solution can’t be expressed in terms of elementary functions, it is more or less easily implemented computationally.

The SD model, then, and its extension by Hughes et al., represent a complete description of an idealized inclusion diffusing in an idealized membrane. Many other models are possible, and have been developed[40, 41], but these are just bells and whistles appropriate for more specific systems, such as curved membranes or inclusions that jut out of the membrane plane. We have found that (2.18) and the HPW model have been adequate to describe our data.

Conclusion

In this chapter I've tried to give a broad overview of the chemistry and physics that inform the structure and material properties of lipid bilayers. Such knowledge will form the basis of any complete understanding of both living membranes and simpler model bilayer systems. But the models I've just presented, and their relation to underlying bilayer structure and phase, are of limited utility if they cannot be tested. In the next chapter I'll turn an experimental protocol that can be used to test models such as the SD or HPW, and in the process yield measurements of the viscosity of bilayers in different phases.

CHAPTER III

MEASUREMENTS AND MICRORHEOLOGY

The picture of membranes developed in chapter two already suggests an experimental approach to measuring bilayer viscosity: measure the diffusion of a membrane inclusion, and use the Einstein relation to calculate viscosity. Passive microrheological experiments follow this suggested protocol¹. In broad strokes, the experiment is that simple. All we require are some small objects that we can embed in a membrane and then image. These objects, termed *tracers* or *probes*, are common biophysical tools. There is, nonetheless, a substantial degree of subtlety in their application. The ways in which such experiments invite complication will become apparent in the following chapter, but for now I want only to explain the analytic tools that microrheology requires- namely, a means of measuring diffusion in a membrane. I will keep the identity of the tracer intentionally generic; you can imagine microbeads or fluorescent proteins. Both of these objects are used in real experiments, but the only crucial requirement is that we are able to *see* the probes, and that they are diffusing.

Since Perrin's experiments in the early twentieth century, the sophistication of methods for measuring diffusion has come a long way. Using (high speed) cameras it is possible to obtain hundred of locations in a diffusing tracer's trajectory in a matter of seconds. These images form a time series from which a diffusion coefficient can be estimated, and from a number of measurements of diffusion we can calculate viscosity. In 2015, then, the task is essentially a task for software.

We'll examine the major steps in a passive microrheology experiment:

1. Locate tracers in successive frames of a recording;
2. Link the tracer locations into tracks, forming a timeseries of tracer displacements;
3. From the timeseries of displacements, estimate the tracers' diffusion coefficients;
4. Use the measured diffusion coefficients to estimate viscosity using appropriate models such as the Saffman-Delbrück or Hughes-Pailthorpe-White models.

¹As opposed to active microrheology, in which membrane inclusions are manipulated through means of some applied force, usually magnetic.

The first two of these steps will be detailed in the first section. Section two on diffusion measurements will discuss the surprisingly non-trivial process of converting tracer displacements to diffusion coefficients. Section three will detail how to obtain membrane viscosity from these diffusion measurements.

Image Processing

Microrheology begins with images of tracers. From an analytic perspective, these images are just arrays of values (integers) corresponding to the measured intensity at a pixel location in a CCD (usually) or CMOS sensor. Unfortunately, the exact value recorded by a sensor suffers from a few complications.

The largest of these is noise. The integers corresponding to a pixel value consist of not just the measured illumination from the tracer, but additionally noise that confounds any task that we could wish to perform. Noise has multiple sources²[42], but regardless of the sources or magnitudes it can generally be modeled by adding a Gaussian random variable to the value of a particular pixel[43]. It is customary and useful to quantify these effects with the Signal-to-Noise Ratio (SNR) of a CCD image. Experimentally this number is easily obtained by measuring the pixel mean value within a portion of the image and the standard deviation of pixel values in the background (thus measuring the variance of the Gaussian random variable)[42].

A second complication concerns the signal itself. This image is built up not just of a direct translation of illumination profile \rightarrow pixel values. Instead, any point source gets “smeared” in its CCD image as a consequence ultimately of the wave nature of light[44]. This smearing is quantified as the microscope’s Point Spread Function (PSF). The image we detect at the CCD is not simply the illumination profile of the object we are imaging, but rather the convolution of that profile with the microscope’s PSF[45]. In practice this means that there is a concrete limit to the amount of contrast we can expect to obtain in any microscope image. Like the SNR, though, the PSF can be measured experimentally. Here the procedure is to image stationary, sub-pixel light sources. The illumination profile measured from such a source allows us to calculate the PSF[46].

²The three main sources of noise in a CCD are dark current (due to thermal generation of electric current), shot noise (variation in the number of photons detected for a given intensity), and read noise (errors in the conversion of light to an electronic signal). These noise sources are in addition any other infidelities in the actual image itself, for instance from optical aberrations.

These are the facts of experimental life. Such issues problematize any direct measurement from microscope images, but one upshot is that by being able to quantify these sources of error we can construct reasonable model microscope images. This means that although it is not always easy to measure experimental uncertainty in microscope images, (for example in determining the precision with which we are locating an object whose true position is unknown), we can get a handle on our precision through simulation. To assess the precision and accuracy of our particle tracking routines, then, we can simulate images in which the true characteristics (such as position) of a feature are known, run the tracking routine, and compare the results to the “true” simulated values.

Particle tracking consists of three main steps: feature identification, localization, and finally trajectory construction. All of these are subject to the experimental uncertainties I just described, but in our systems identification and trajectory linking are much more trivial than localization. This is more or less due to the nature of the experiment: modern fluorophores are almost miraculous in brightness and longevity, and so tracers can generally be identified through simple thresholding³ and linked into tracks using a simple nearest neighbor algorithm⁴. But this is also due to the nature of the task. Identification and linking are essentially binary operations: we want to know if a particular region of an image forms part of a tracer or not, if a series of tracer locations form a track or not. Localization, on the other hand, returns a quantitative measurement, the probe’s location. This means that while localization schemes equivalently simple (or “dumb”) as thresholding can be pursued, metrics of success have allowed innovators to increase performance. Sophistication in this regard goes a long way. Given all of the uncertainty in measurement, and the digitized, discrete nature of the measurement itself, one could be forgiven for assuming that we can only broadly give the location of a tracer. Actually, sub-pixel resolution is readily achievable, and good localization algorithms approach the theoretical limit in precision for an unbiased estimator (the Cramer-Rao lower bound)[44].

³In practice, we do process images before identifying features. A bandpass filter can greatly reduce error in feature identification by limiting noise on the lengthscale of the features we wish to identify. Still, stochastically bright pixels will often produce several illumination peaks within the vicinity of a true feature, leading to multiple feature identifications even when just a single object is present. This effect can be limited by dilating these illumination peaks to the size of the feature we are looking for; overlapping peaks can then be identified as a single object.

⁴In this algorithm, we look for the tracers that agree that they are closest to each other in successive frames, and link these tracers as the time series of a single object. This task is made simple in microrheology due to an unrelated experimental requirement that probes be disperse.

In Parthasarathy group, we use two different localization techniques, both of which are essentially optimal. For small, point-source like objects (in our experiments, paired microscale beads) we can use a radial symmetry based approach[45]. For more extended objects (phase separated domains), we use the ponderously slow Gaussian Maximum Likelihood Estimation (Gaussian MLE).

The first of these approaches, radial symmetry localization, works by exploiting the fact that, for a radially symmetric illumination profiles, lines drawn perpendicular to profile's gradient will intersect at the profile's center. Of course, in noisy images such gradient lines will not neatly intersect in just one location; nonetheless we can identify the center of the object with the point that minimizes the distance between all such lines⁵. This approach is surprisingly robust: Fig. 6 shows the localization precision obtained from radial symmetry localization as a function of SNR for simulated *ellipsoidal* tracers. Even though ellipsoids are obviously not radially symmetric, the algorithm performs as well as or better than any of other localization technique that we tested. Furthermore, it has a swift execution time. This is because the radial center can be calculated algebraically, in sharp contrast to (most) other localization techniques, which require iterative fitting of parameters.

While radial symmetry localization works well for small objects, we find that it does not perform well with larger, extended objects such as phase separated domains. For such objects, we resort to Gaussian MLE fitting. This technique executes more slowly by over an order of magnitude, but achieves better precision and accuracy for such objects. It works by maximizing the likelihood function, which gives the probability of observing a given data set given a set of parameters, for a Gaussian illumination profile. Estimation of this variety is a powerful analytic/computational technique, and furthermore it is an incredibly general, "turn the crank" procedure. A good discussion of MLE and other estimation schemes can be found in Ref. [47].

In a microrheology experiment, these steps are often all of the image processing that is required. After we have completed these steps (feature identification, localization, linking), we will be in possession of a time series of probe displacements. It is from this data that we calculate diffusion coefficients.

⁵For high accuracy, it is also necessary to weight different lines' contribution to this minimization.

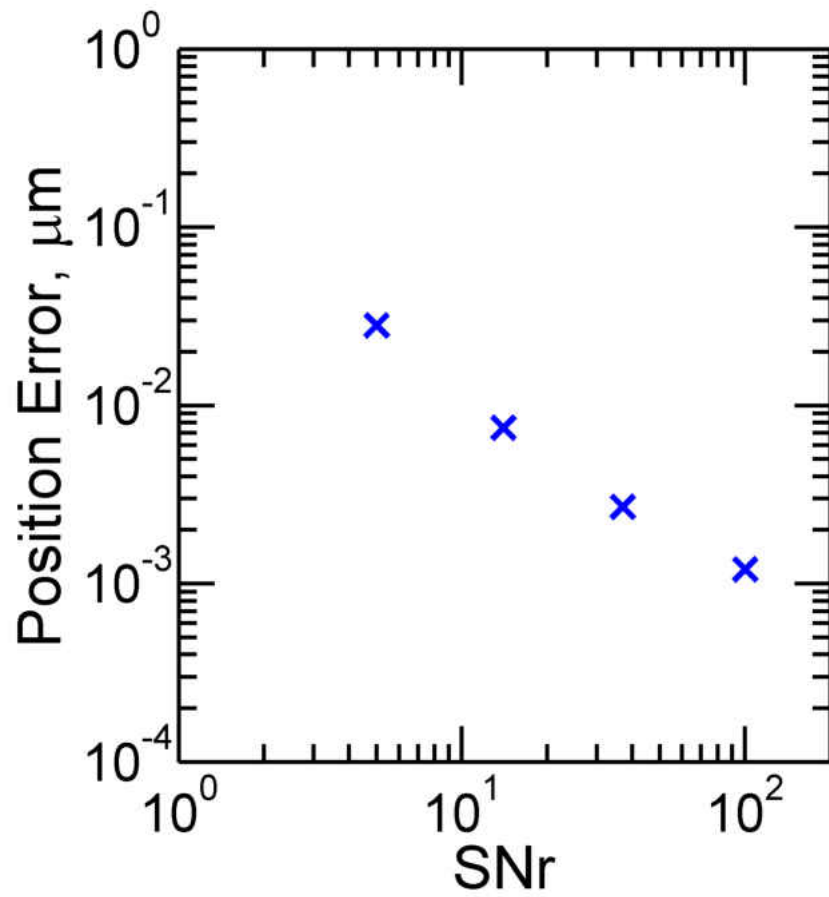


FIGURE 6. Simulated localization error vs. SNR for elliptical tracers localized using the radial symmetry based approach.

Diffusion Measurements

The canonical diffusion scaling relation states that

$$Dt = \langle \Delta \mathbf{x}^2(t) \rangle, \quad (3.1)$$

that a diffusing particle's Mean Square Displacement (MSD), not simply the mean displacement, scales linearly with time. Equation (3.1) is extremely useful, and has afforded an enormous degree of insight in to biological function⁶. It suggests a method for estimating a particle's diffusion coefficient. Simply take the measured displacements from the particle's trajectory, square, and fit successively further temporally separated displacements (between frames 1 and 10, say, instead of 1 and 2) to a line. Despite its utility in other contexts, however, (3.1) does *not* provide a good estimate of D . The problem is that displacements $\Delta \mathbf{x}(t)$ are correlated. An easy way to see this is to note that we are recycling measurements to obtain this estimate. Since we build up a particle's mean square displacement as a function of time by considering displacements between frames separated by successively larger times, we end up using the particle's position in most frames to calculate not just $\mathbf{x}(t_{n-1}) - \mathbf{x}(t_n)$, but also $\mathbf{x}(t_{n-2}) - \mathbf{x}(t_n)$ and $\mathbf{x}(t_{n-3}) - \mathbf{x}(t_n)$, etc., where n denotes a frame number. This has the unexpected affect of *reducing* the precision of an MSD based estimate as more time lags are included⁷[48].

This fact is not widely appreciated. Luckily, while an MSD based estimate is imprecise, it is still unbiased. Nonetheless better estimators exist. We currently make use of a Covariance based Estimator (CVE)[48]. This essentially optimal estimator takes the form

$$D = \frac{\langle \Delta \mathbf{x}_n^2 \rangle}{2\Delta t} + \frac{\langle \Delta \mathbf{x}_n \Delta \mathbf{x}_{n+1} \rangle}{\Delta t}. \quad (3.2)$$

⁶For example, simple diffusive scaling explains why bacteria don't need molecular motors, and why their swimming strategies are optimized for finding high food concentrations only, to name just a few examples.

⁷Clever MSD based estimates can mitigate this problem to certain extent, but suffer from unwieldiness and are in general difficult to analytically characterize.

Furthermore, the formalism used to develop the estimator also supplies an associated estimate of uncertainty in localization

$$\sigma^2 = R \langle \Delta x_n^2 \rangle + (2R - 1) \langle \Delta x_n \Delta x_{n+1} \rangle \quad (3.3)$$

and the estimate of D

$$\text{var}(D) = D^2 \left[\frac{6 + 4\xi + 2\xi^2}{N} + \frac{4(1 + \xi)^2}{N^2} \right], \quad (3.4)$$

where $\xi = \sigma^2 / (D\Delta t) - 2R$, N is the total number of frames, and R is a numerical constant related to the camera shutter (= 0.6 if the shutter is left open for the duration of data acquisition, which is normal).

Parameter Estimation

From the estimates of diffusion coefficients so obtained, we wish to extract a measurement of the fluid properties of the material in which the tracers are included. Inasmuch as we model the bilayer as a simple fluid, we are particularly interested in measuring viscosity, although in principle any of the techniques I will discuss here would be equally suited to the examination of other material properties given other models. Even in the Saffman-Delbrück model

$$b_T = \frac{1}{4\pi\eta} \left(\log \frac{\eta}{\eta_w a} - \gamma \right),$$

the simplest model we have for membrane viscosity, we are confronted with a non-algebraic dependency of viscosity on diffusion coefficient. The greater complication is that our measurements of D for every tracer contain some degree of uncertainty. As for the tracer locations, and the diffusion coefficient itself, some technique for estimating the viscosity is needed.

One reliable and fairly general technique utilizes the χ^2 test statistic. For a set of measurements y_i that we are attempting to describe with some model $f_i(\alpha; x_i)$ with fit parameter

α , such that $y_i = f_i(\alpha; x_i)$, this statistic is given by

$$\chi^2(\alpha) = \sum_{i=1}^N \left(\frac{y_i - f_i(\alpha; x_i)}{\sigma_i} \right)^2, \quad (3.5)$$

where σ_i being the uncertainty in the measured value y_i . Even outside of parameter estimation, the χ^2 value of experimental data with respect to a specific model is useful: it quantifies how well the data fit the model under consideration. Without too much work χ^2 values can be converted to p values. With even less work one can compare χ^2 to N , the number of observations in the data set. The difference of these values should be the same as the number of constraints in the model; roughly, how many parameters within the model were calculated from the experimental data. Actually, it is more usual to make this quantitative assessment with respect to the *reduced* χ^2 value, given by $\tilde{\chi}^2 = \chi^2 / (N - c)$, where c is the number of constraints. In this case, we expect $\tilde{\chi}^2 \approx 1$.

A word of warning. (3.5) assumes that the data being considered (the y_i) are normally distributed around their actual (theoretical) values[49]. This is one reason that binning experimental data is useful: the values in a bin give the distribution of the data around the expected model parameter⁸.

To use (3.5) in order to estimate a model parameter, we compare the experimental data to the model value for that data calculated assuming a particular parameter value α . We then search for the value of α that minimizes the χ^2 statistic over the entire data set. Several algorithms for finding this minimal value exist[50]. For the computers of 2015, even the dumbest, most computationally expensive method, the grid search, can be completed fairly quickly, even for models as complex as the HPW model of diffusion in a membrane. In this method, we simply incrementally check all of the possible values in a range of interest, and then equate our estimate with the smallest value so calculated. The grid search, though expensive, guarantees that we will find the minimal χ^2 value, provided the increments in our search are small enough.

This methodology will retrieve an estimate of a model parameter; of course, we would also like to obtain uncertainty in our estimate. For χ^2 minimization, the exhaustiveness of the

⁸The normality demand is not always easy to quantify in this way, especially when experimental limitations produce bins with limited numbers of data points. A seemingly cavalier but widely used rule of thumb states that each bin contain at least 5 data points.

grid search is in some ways an added virtue in this respect. In the right circumstances⁹, the distribution of χ^2 around its minimum can be used to calculate this uncertainty. However, with even average computers, computation is now affordable enough that we can resort to general approaches that have no regard whatsoever for how the data is distributed. One such approach is *jackknife resampling*, in which we obtain a new data \bar{y}_i by removing a single measurement[51]. In this way we can generate N new data sets, and from each we can then generate a new jackknife estimate of the fit parameter $\bar{\alpha}$. The variance of these jackknife estimates $\bar{\alpha}$ provide an estimate of the uncertainty in our estimate according to

$$\sigma^2 = (N - 1) \sum_{i=1}^N \frac{(\bar{\alpha}_i - \alpha)^2}{N}. \quad (3.6)$$

Conclusion

These are the analytical and computational techniques that we've used to obtain our measurements of membrane viscosity. I've yet to talk about the experimental techniques that are required to perform such an experiment. This will be the topic of the next chapter, in which I will also present the results from two such experiments.

⁹For instance, that $\chi^2(\alpha)$ is locally parabolic- not always a particularly good assumption with models as non-linear as HPW.

CHAPTER IV

EXPERIMENTS AND RESULTS

Introduction

In order to actually employ any of the experimental techniques that I have discussed, we must choose an experimental system to examine. Like most things in life, there is no perfect model membrane system, and any selection will entail complications or limitations to the experimentalist. The degree to which these complications are assessed and characterized can make an experiment that would otherwise yield precise measurements inconclusive, or vice versa. The first experiment I'll present is a good example of dealing with features and complications that are often glossed over. This chapter includes material coauthored with Sarah Kurihara, Kathleen Brennan, Matthew Wozniak, Matthew Reyer and Raghuvver Parthasarathy.

Rotating Tracers

Though measurements of lipid and protein diffusion coefficients are routine, it is difficult to determine membrane viscosity, the fundamental material property that describes fluid response, from such measurements. This difficulty can be ascribed in part to ignorance of the effective size of diffusing bodies. The approach we describe here uses measurement of both the translational and rotational diffusion coefficients of membrane-anchored tracer particles to provide, via simple analysis, precise and robust values of viscosity as well as effective tracer radii. The method is generally applicable to membranes of different compositions and geometries, and allows tests of theoretical models of membrane hydrodynamics. Moreover, it enables discovery of rheological effects induced by membrane proteins. We provide the first demonstration that a protein involved in generating membrane curvature also has a large impact on the effective in-plane membrane viscosity, a finding that would have been difficult to uncover with existing techniques.

Diffusion in two dimensions is inherently non-trivial due to the long range of flow fields. Saffmann and Delbrück (SD) showed that hydrodynamic coupling between the 2D membrane and the bulk 3D fluid results in well-defined diffusive behavior within the membrane[38]. According to this model, the rotational and translational drag coefficients b_R and b_T , respectively, for a disk-like

membrane inclusion of radius a are given by

$$b_T = \frac{4\pi\eta_m}{\ln(2\epsilon^{-1}) - \gamma}, \quad (4.1)$$

$$b_R = 4\pi\eta_m a^2; \quad (4.2)$$

where γ is Euler's constant, η_m is the two-dimensional membrane viscosity and $\epsilon = 2\eta_w a/\eta_m$ is a dimensionless number relating a , η_m , and the bulk 3D viscosity η_w . The diffusion coefficients follow from the drag coefficients via the Einstein relations $D_{R,T} = k_B T (b_{R,T})^{-1}$, where k_B is Boltzmann's constant and T is the temperature. The SD model is valid in the limit of small ϵ , corresponding to membrane inclusion radii that are small compared to the ratio of the 2D membrane viscosity to the 3D bulk viscosity. Hughes, Pailthorpe and White (HPW) extended the SD model to arbitrary ϵ [39]. The full HPW model cannot be condensed into simple equations, but can be evaluated computationally. Both the SD and HPW models describe diffusion in a planar membrane. However, membrane inclusions may generate distortions of the membrane's shape[52–54]. A recent model by Naji, Levine and Pincus (NLP)[40] considers protrusions as generating additional dissipation in the bulk fluid, leading to an effective translational drag:

$$b_{T,\text{eff}} = b_T + c\eta_w a (b_T)^{-1}. \quad (4.3)$$

The parameter c is, roughly, the ratio of the volume of bulk fluid displaced by the membrane deformation to a^3 . High values of c , then, indicate that the presence of the membrane inclusion is leading to large out of plane membrane deformations, while low values correspond to relatively smaller membrane deformations.

In conventional microrheology, the viscosity of Newtonian fluids is typically extracted from measurements of (just) the translational diffusion coefficient D_T of tracer particles [55, 56]. This diffusion coefficient, the temperature and the tracer's radius can then be used to determine the viscosity of the fluid by using an appropriate model. For 3D fluids, the radius a is typically taken to be the tracer particle radius, though there are situations in which this is a poor assumption due to interactions between the particle and its surroundings[57]. For membranes, it is especially dangerous to assume that the effective radius of the diffusing object is identical to the radius of a membrane-bound tracer. Unless using phase-separated lipid domains as tracers[31, 34, 35], in

which case the tracer radius equals the domain radius, the tracked particles must be peripherally bound to the lipid bilayer, for example by a protein-lipid linkage. The number of lipid links is generally not easily controlled, and could range from one lipid (an area of approximately 70 \AA^2 [58]) to an upper limit set by the tracer surface area. Moreover, it would not be surprising if the binding of a colloidal particle induced distortions of the membrane topography, further impacting the effective size of the diffusing object. We address these issues by measuring the rotational diffusion coefficients (D_R) of our membrane-bound tracers in tandem with their translational diffusion coefficients (D_T). These two measurements allow determination of the two unknown quantities, namely the inclusion radius a and the membrane viscosity η_m , via the SD, HPW or NLP relations.

Experimentally, we make use of planar bilayers spanning apertures in supports, also known as black lipid membranes (BLMs). The geometry conveniently confines tracer motion to the focal plane of our microscope, and the lack of a support eliminates frictional coupling between the membrane and solid or polymeric substrates[59]. The bilayers are formed using Langmuir-Schaefer deposition[60] from lipid monolayers at air-water interfaces, composed of a majority (typically 98%) of a single lipid species, for instance 1,2-dioleoyl-sn-glycero-3-phosphocholine (DOPC), with a small percentage of fluorescent lipid probes for visualizing the membrane (Texas Red DHPE) and lipids with biotinylated headgroups. The membranes span $100 \mu\text{m}$ diameter apertures in hydrophobically-coated gold transmission electron microscope grids. This diameter is large compared to the physical tracer size, the effective tracer radii noted below, and the length scale set by the ratio of (expected) 2D to 3D viscosities $\eta_m/\eta_w \approx 1\mu\text{m}$.

The biotinylated lipids in the membrane are bound by neutravidin-coated fluorescent microspheres of radius 100 nm . These in turn bind 100 nm biotinylated fluorescent microspheres (Fig. 7), forming an extended unit whose orientation as well as position can be discerned in CCD images. Fluorescence images of beads were captured at 10 to 40 frames/second, and analyzed to give particle locations and orientations with an estimated precision of 1.2 nm and 0.022 radians , which yield average uncertainties of $6.3 \text{ nm}^2/\text{s}$ for D_T and $7.2 \times 10^{-4} \text{ rad}^2/\text{s}$ for D_R , both of which are negligible compared to the statistical spread in the data. All experiments were carried out at room temperature ($24 \pm 1 \text{ }^\circ\text{C}$).

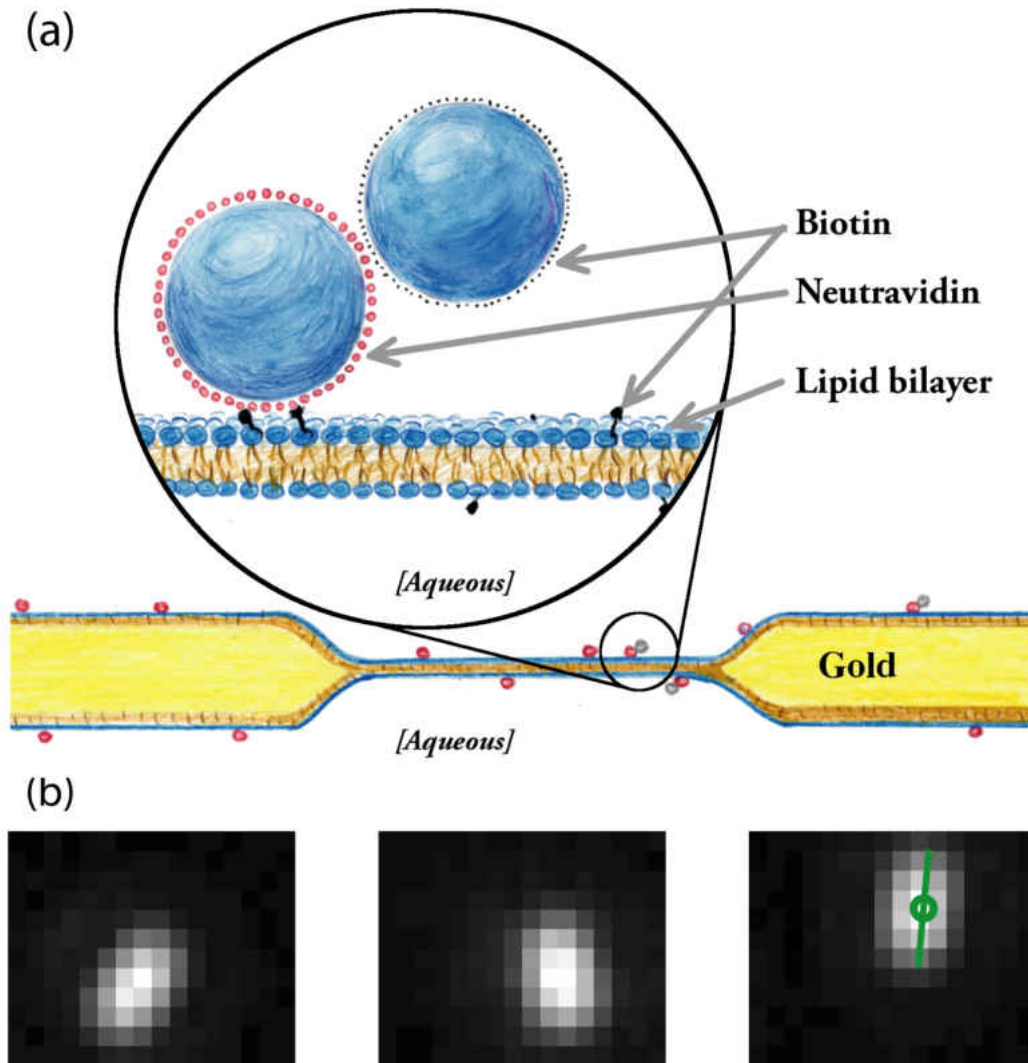


FIGURE 7. Experimental setup. (a) Schematic of a membrane spanning an aperture. Fluorescent microspheres are associated with the membrane via a protein linkage, including some that are also bound with other microspheres to form the non-spherical tracers considered in the text. (b) Fluorescence images of one microsphere pair, separated by 0.3 seconds. Both rotational and translational motion are apparent as the tracer thermally diffuses. The final image shows the best-fit center and orientation of the tracer. Scale: $0.123 \mu\text{m}/\text{pixel}$.

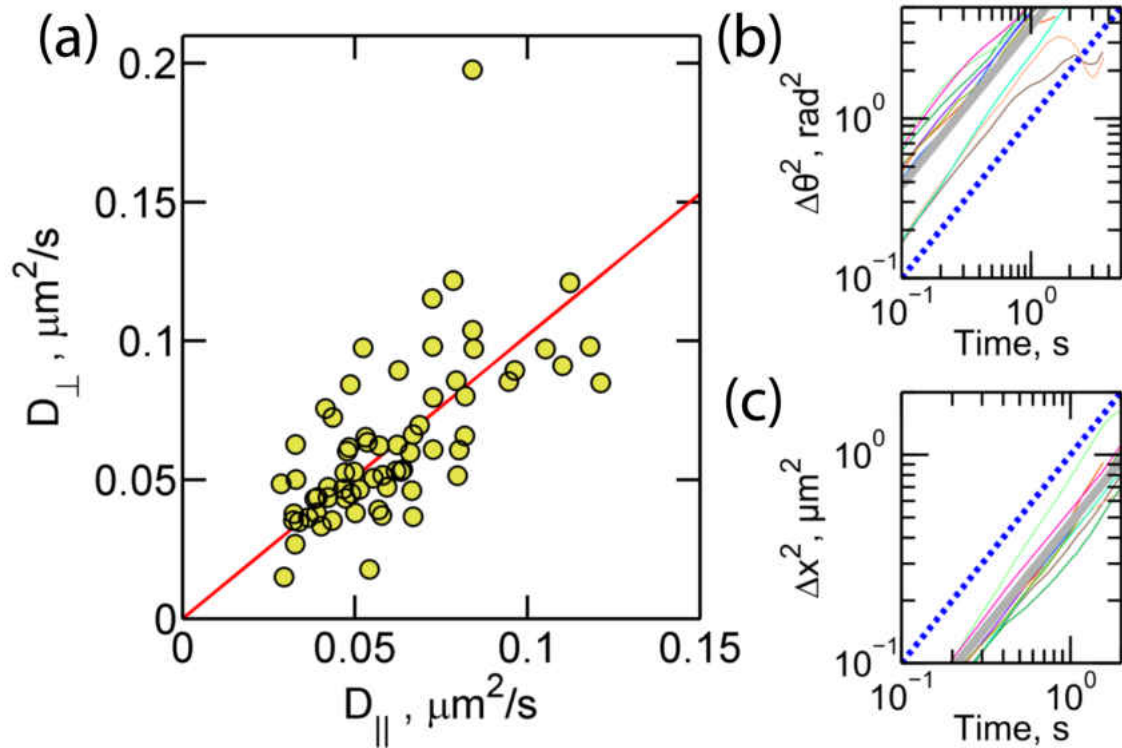


FIGURE 8. Diffusive behavior of tracers at DOPC bilayers. (a) Diffusion coefficients for motion parallel (D_{\parallel}) and perpendicular (D_{\perp}) to the tracer long axis. The best fit line, shown in red, has slope $B = 1.03 \pm 0.04$, indicating isotropic diffusion. (b) and (c): Translational and angular mean square displacements versus time for several tracers. The average is shown as a thick gray line, while a dotted line with slope = 1 (expected for purely diffusive motion) is shown as a guide to the eye.

The small tracer size helps ensure that tracer motion is dominated by the mechanics of the membrane rather than dissipation in the bulk fluid. For an expected membrane viscosity of, roughly, $\eta_m \approx 3 \times 10^{-9}$ Pa·s·m[61], the Stokes drag for translation in the bulk for a bead of radius ≈ 100 nm is an order of magnitude smaller than the Saffman-Delbrück drag b_T for a 100 nm disk; the same relative scale holds for rotation. Furthermore, with the above values, the dimensionless size parameter $\epsilon \approx 0.1$. Therefore, though we perform calculations using the full HPW model, we expect our system to occupy the regime of validity of the SD relations. Note also that, though the HPW and SD models describe the diffusion of cylinders incorporated into membranes, the diffusion of membrane inclusions in this regime is largely insensitive to protrusions[62].

We are able to observe the translational and rotational diffusion of membrane-anchored particle pairs (Fig. 7). The elongated form of the composite paired tracer does not bias the tracers' trajectories. Decomposing the translational diffusion into components along (D_{\parallel}) and perpendicular (D_{\perp}) to the ellipse major axis, we find that $D_{\parallel} = BD_{\perp}$ with $B = 1.03 \pm 0.04$ (Fig. 8a), implying that the diffusing object can be treated effectively as an isotropic membrane inclusion. As we would expect from the dominance of the membrane drag compared to the bulk noted above, and from the lack of binding between the secondary beads and the bilayer, it appears that the tracer motion is dominated by the diffusion of a region of anchored lipids diffusing within the bilayer and not by the size and shape of the tracer pair. We find that the mean-squared translational and rotational displacements are each linear in time over experimentally accessible time-scales (Fig. 8b), indicative of Newtonian fluid dynamics, and thereby allowing application of the SD and HPW models.

We observe a spread of D_T and D_R values within and among lipid bilayers of identical composition. Applying the SD relations yields a wide range of effective radius (a) values (Fig 9, inset). The mean inclusion radius, 170 nm, is orders of magnitude larger than the radius of single lipids (0.5 nm[58]), and is about twice as large as the 100 nm radius of the primary membrane-linked microspheres. The distribution shows a long tail with some effective radii exceeding 500 nm. On the other end, we do not find radii much smaller than 50 nm, indicating that each neutravidin-coated microsphere is anchored to the membrane at several binding sites.

Each of the models of membrane viscosity we consider describes a relationship between D_R and D_T for a given viscosity. This relationship can be used to construct contours of constant

viscosity on D_R - D_T axes (Fig. 9). If a particular model describes the D_R and D_T measurements well, the measured values for individual tracers should collapse on to one of these contours. We find that the SD model is a fair fit to the data (Fig. 9), yielding a best-fit viscosity of $15.3 \pm 3.4 \times 10^{-9}$ Pa·s·m for DOPC bilayers. The goodness of fit (reduced χ^2) of the SD model to our data is 0.41. The full HPW model performs similarly, with a viscosity of $15.9 \pm 2.3 \times 10^{-9}$ Pa·s·m, and reduced $\chi^2 = 0.48$. It is reasonable to speculate that our tracers may deform the membranes to which they are associated. We therefore also fit our data to the NLP model. This achieves a closer fit (reduced $\chi^2 = 0.28$), with viscosity $13.1 \pm 2.6 \times 10^{-9}$ Pa·s·m, but at the expense of the additional parameter c . One would expect $c^{1/3}$, the effective rescaling of the radius due to deformation, to be of order 1. We indeed find that $c^{1/3} = 3.0 \pm 0.5$.

To evaluate the robustness of our approach for measuring membrane viscosity, we examined another lipid that, like DOPC, is in a fluid (L_α) phase at room temperature: 1,2-di-O-tridecyl-sn-glycero-3-phosphocholine (13:0 PC)[63]. Fluorescence recovery after photobleaching (FRAP) measurements (performed as in [64]) give similar lipid translational diffusion coefficients for the two species: $D_{\text{lipid}} = 3.4 \pm 2.3 \mu\text{m}^2/\text{s}$ for 13:0 PC bilayers and $D_{\text{lipid}} = 4.1 \pm 1.2 \mu\text{m}^2/\text{s}$ for DOPC bilayers. Unlike DOPC, 13:0 PC is a saturated lipid, and has a shorter acyl chain length (13 carbon atoms, compared to 18 for DOPC). Viscosity measurements for 13:0 PC give $14.7 \pm 6.9 \times 10^{-9}$ Pa·s·m using the HPW model ($\chi^2 = 3.4$), or $10.4 \pm 4.8 \times 10^{-9}$ Pa·s·m ($\chi^2 = 1.8$) using the NLP model ($c^{1/3} = 3.8 \pm 1.3$). These viscosities are similar to those we measure for DOPC.

Notably, using lipid radius $a = 0.5$ nm and $D_{\text{lipid}} = 3 \mu\text{m}^2/\text{s}$ gives a membrane viscosity of 1×10^{-10} Pa·s·m, two orders of magnitude smaller than that measured above. This is not surprising; it has long been known that hydrodynamic treatments fail at molecular scales, and that diffusing lipids experience an effectively lower viscosity than do embedded proteins or other larger objects[21].

The viscosity values we observe are larger than those reported for fluid phases in membranes exhibiting cholesterol-dependent phase separation, derived by examining the diffusion of domains of one phase in another [31, 34, 35], or by measuring the shape fluctuations of domain boundaries [32]. For liquid-disordered (L_D) phases, values of $(3.3 \pm 1.1) \times 10^{-9}$ [61] and $(5.4 \pm 1.4) \times 10^{-9}$ [65] Pa·s·m have recently been reported. There are fewer measurements

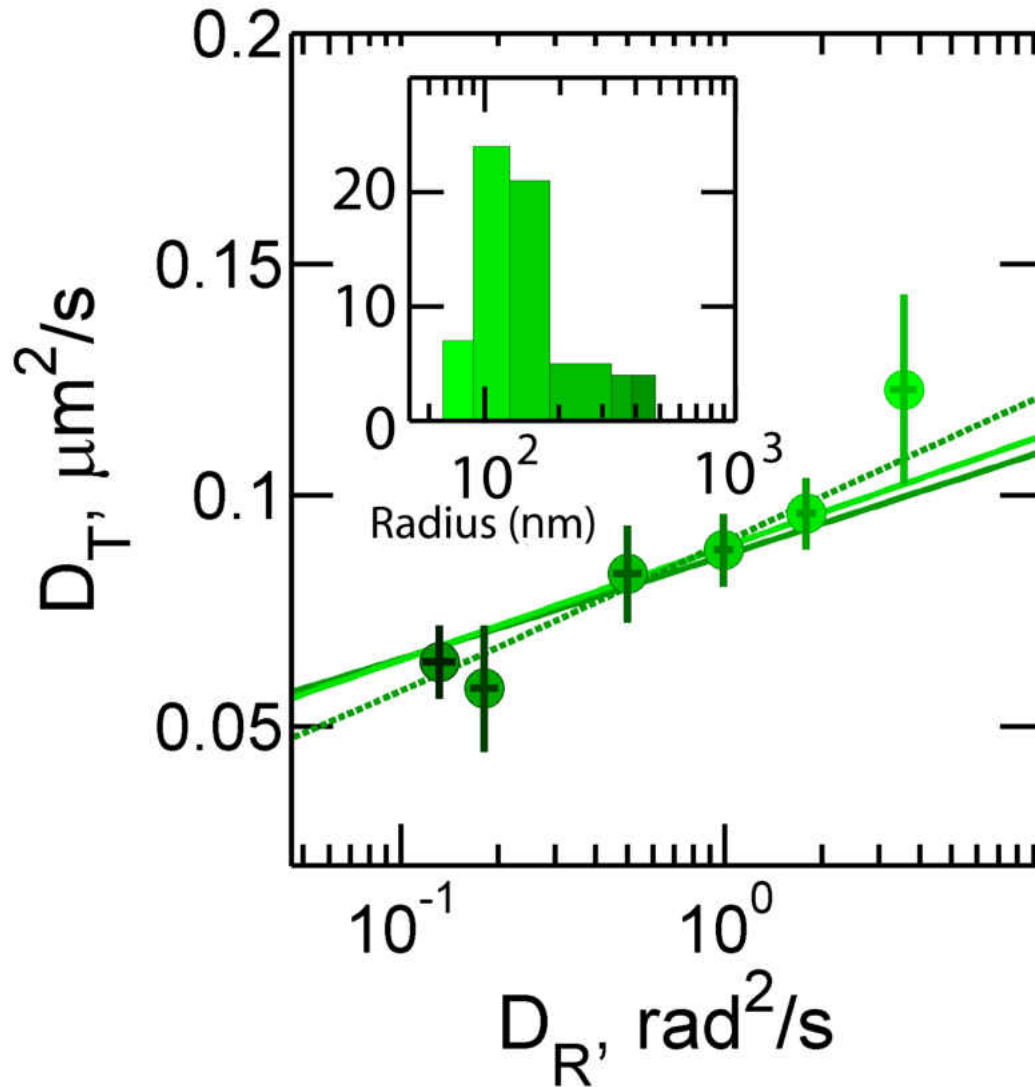


FIGURE 9. Effective inclusion radius and viscosity of a DOPC bilayer. (Main Panel) Translational and rotational diffusion coefficients. Each data point is the average of 4 to 24 individual tracer measurements, with the error bars indicating the standard deviations. Decreasing inclusion radius size is indicated by progressively lighter shades of green. The curves are best-fit constant-viscosity contours determined by the SD (light green, solid), the HPW (dark green, solid) and NLP (dark green, dashed) models. (Inset) Histogram of effective tracer inclusion radii on log-linear axes. The bins correspond to the data points in the main panel, with radii obtained using the SD model, and placed such that the left-hand edge of the bin corresponds to the largest inclusion radius in its set. Though peaked near the microsphere radius of 100 nm, much larger inclusion radii are evident.

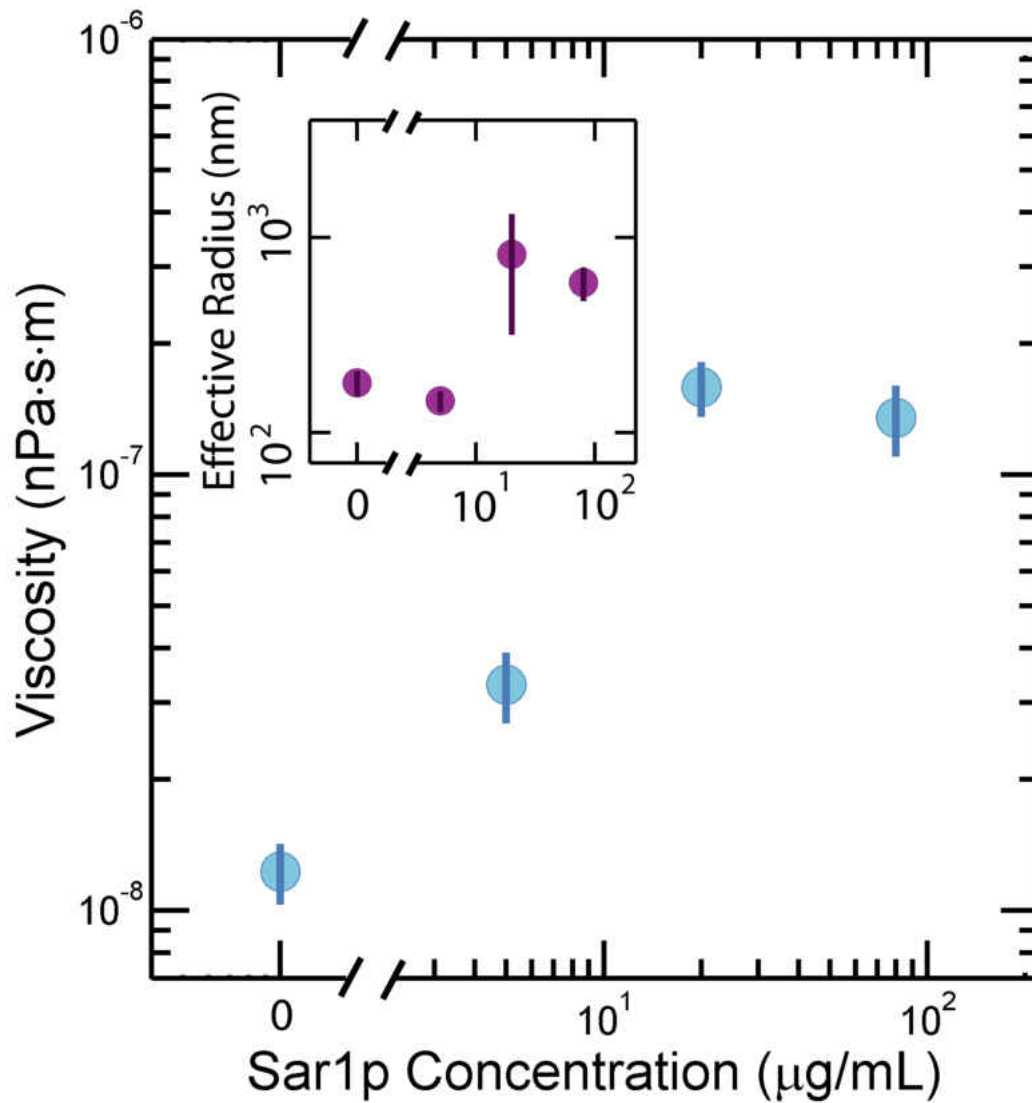


FIGURE 10. Membrane viscosity measured at different concentrations of the trafficking protein Sar1p on a log-log scale. The plot shows the mean and standard error of viscosity values determined by fitting individual paired-tracer diffusion coefficients to the HPW model, at each protein concentration examined. Inset: The effective radius for the same data, also on a log-log scale.

of the viscosity of homogeneous (not phase-separated) fluid bilayers, and these, prior to the method introduced here, involve complex, model-dependent analyses. Dimova *et al.* examine the gravity-driven fall of a microparticle along the surface of a giant lipid vesicle, the hydrodynamic interactions between which are computed to give a two-dimensional viscosity of $(3 \pm 0.9) \times 10^{-9}$ Pa-s-m for SOPC (1-stearoyl-2-oleoyl-sn-glycero-3-phosphocholine)[66]. For DOPC, which differs by a single double bond in one of the eighteen-carbon acyl chains, Herold *et al.* report $(5.9 \pm 0.2) \times 10^{-10}$ Pa-s-m based on the Brownian motion of absorbed DNA, whose radii of gyration are estimated from comparisons of their diffusion coefficients with those of colloidal tracer particles[67]. There are several possible reasons for the $\approx 10\times$ difference between the viscosity that we measure and those reported for other fluid membranes: multi-component, phase separated membranes may simply have a lower viscosity than the phosphatidylcholine membranes used in this study; the BLMs examined here may not consistently be pure lipid bilayers, due to retention of solvent during their formation; membrane tension in the edge-adhered BLM geometry may differ considerably from that of lipid vesicles, altering the membrane viscosity. While developing experiments to investigate these topics is likely to yield future insights, a question of greater importance is whether our approach can reveal *alterations* in membrane rheology driven by membrane-active proteins.

Proteins that are actively involved in reshaping membranes, generating curvature in contexts such as cargo trafficking, filopodial extension, and mitosis[68–70], form a particularly interesting class of macromolecules in which to uncover previously unknown couplings to membrane viscosity. We focus on the vesicle trafficking protein Sar1p, a 21 kDa protein with an N-terminal amphipathic alpha helix that anchors it to lipid membranes[71–73]. Prior experiments have shown that Sar1p dramatically lowers the bending rigidity of lipid bilayers [74, 75], leading to the open question of whether its influence also alters the in-plane viscosity. Measuring tracer diffusion in BLMs with the same endoplasmic-reticulum-mimic lipid composition and similar range of Sar1p concentration ($[\text{Sar1p}]$) as previously examined[74–76], we find a large drop in diffusion coefficients as a function of $[\text{Sar1p}]$. Separating the roles of effective radius and membrane viscosity, we find an increase in a of $\approx 4.5\times$, and a dramatic increase in η_m of more than an order of magnitude (Fig. 10). Notably, the lipid diffusion coefficient is unaffected by Sar1p [77], again highlighting that the viscosity experienced at molecular length scales can differ greatly

from its effective value for larger objects. While a mechanistic explanation of Sar1p’s influence on measured viscosity is beyond the scope of this work, we note that Sar1p’s reduction of the membrane bending modulus leads to enhanced topographic fluctuations [75], which may obstruct lateral motion. Notably, budding transport vesicles (formed by Sar1p and other proteins) are of similar 10-100 nm size as our tracers and their effective radii, suggesting that Sar1p’s effect on viscosity at this scale can affect the dynamics of vesicle trafficking.

The results presented above demonstrate a microrheological method that can robustly be applied to fluid membranes, including membranes with bound proteins. Furthermore, since our method requires only that the membrane incorporate biotinylated lipids to construct a tracer linkage, different model systems (e.g., supported bilayers, multilayers, and giant unilamellar vesicles) could be studied using the same approach. An important conclusion that can be drawn from our measurements is that the linkage between membrane and tracer can be non-trivial. Finally, we note that our discovery that the trafficking protein Sar1p dramatically increases large-scale membrane viscosity opens the door to a wide range of studies on the impact of proteins upon membrane rheology.

Two-point Microrheology

Introduction

Many of the most precise measurements of lipid bilayer viscosity have used passive microrheology, in which the Brownian trajectories of membrane-anchored particles or of lipid domains in the bilayer are recorded and analyzed to reveal insight into the fluid properties of the sample [34, 35, 78]. While powerful, all such studies to date have made use of single-point methods, in which the statistics of individual tracer motions are analyzed, which report on the local environment of the tracer and hence may not be representative of global characteristics, perhaps due to the influence of the tracer itself.

The methodology of two-point microrheology compliments single-point techniques by considering the correlated displacements of pairs of particles. This extends the length scale examined from the tracer radius to the separation distance between tracer pairs, and is therefore sensitive to the separating medium in addition to the individual tracer neighborhoods [79–82]. Disparities between two-point and single-point microrheology, then, demonstrate length-scale

dependent effective viscosities. For a cellular membrane, such length-scale separation could imply that the viscosity relevant for protein diffusion, say, would be different than the viscosity relevant for large scale membrane deformations.

Two-point microrheology has been applied to a wide variety of three-dimensional materials [79, 83, 84], and has been extended both theoretically and experimentally to two dimensional fluids. Levine and MacKintosh have derived the response functions that characterize a membrane embedded in a three dimensional fluid, providing explicit forms for interparticle correlation functions that can be compared to measured correlations [85]. Weeks and co-workers have used two point microrheology with colloidal microspheres as tracers to examine thin soap films as well as proteins at an air-water interface, quantifying the two dimensional viscosity and establishing the hydrodynamic response functions of these systems [86–88]. To date, these pioneering studies have been the only published reports of two point microrheology of two dimensional fluids, leaving open the question of what two-point analysis will reveal for lipid membranes. In particular it is unknown, prior to the studies reported here, whether simple viscous fluid models are adequate to describe correlated diffusion of membrane inclusions, and if so, whether the reported viscosity will be the same as that shown by single-point methods.

We examined the rheology of giant unilamellar vesicles (GUVs) exhibiting cholesterol-dependent phase separation into coexisting liquid phases. Such systems can be broadly controlled to tune the degree and scale of compositional heterogeneity. Furthermore, phase separated bilayers are well characterized model systems [89], and, importantly, have been studied using single point microrheology since phase separated domains themselves can be used as tracers that report the viscosity of the majority phase [34, 61].

Materials and Methods

Giant Unilamellar Vesicle Composition and Preparation

We formed GUVs by electroformation [90] in 0.1 molar sucrose, and used the same solution for the exterior environment in our experiments. The diameters of the vesicles examined were in the range 50-100 μm . We considered five different GUV compositions with differing fractions of DPPC (1,2-dipalmitoyl-sn-glycero-3-phosphocholine), DOPC (1,2-dioleoyl-sn-glycero-3-phosphocholine) and cholesterol. All lipids were purchased from Avanti Polar Lipids. Vesicles

with such compositions readily partition into liquid-ordered (L_O) and liquid-disordered (L_D) domains [29, 30, 61, 65, 89]. This phase separation can be observed experimentally through inclusion of a small amount of Texas Red DHPE, a fluorescent lipid probe that preferentially partitions into the L_D phase (Fig. 11). In our experiments, we formed GUVs with 1 mol% Texas Red DHPE. Control experiments using a lower probe concentration (0.2 mol%) showed similar domain diffusion coefficients, but poor signal-to-noise ratios prohibited precise assessments of viscosity.

Fluorescence Microscopy and Domain Tracking

We recorded epifluorescence images at 10-40 frames per second with a Hamamatsu ORCA CCD camera on a Nikon TE2000 inverted fluorescence microscope with a 60X magnification objective. All measurements were made at room temperature (296 K).

We identified phase separated domains in images by intensity-based thresholding and estimated domain centers by fitting two-dimensional Gaussian profiles using maximum likelihood estimation. From tracking simulated images with similar signal-to-noise characteristics, and from the statistical assessment of Ref. [48] (see below), we estimate our localization error to be less than $0.07 \mu\text{m}$. This localization uncertainty contributes to the uncertainty in measured diffusion coefficients and correlations. Domain boundaries were determined using a bilateral filter [91]; the enclosed area was used to determine the domain radius. Uncertainties in the domain radius due to growth and bulging of domains out of the membrane plane have negligible effects on the assessed viscosities. We considered only domains that are located within at most $1/3$ of the vesicle radius from the GUV pole, as these appear in-focus in images, and only small components of their motion are perpendicular to the focal plane. Furthermore, we selected only domains that were continuously imaged for at least one hundred frames; this ensures sufficient statistics to characterize domain diffusion (see below). We linked domain positions into trajectories using a nearest neighbor linking algorithm. This process yields a time series of domain positions for several domains per GUV that can be analyzed to obtain diffusion coefficients and other statistics. The number of domains per GUV ranged from three to over fifty.

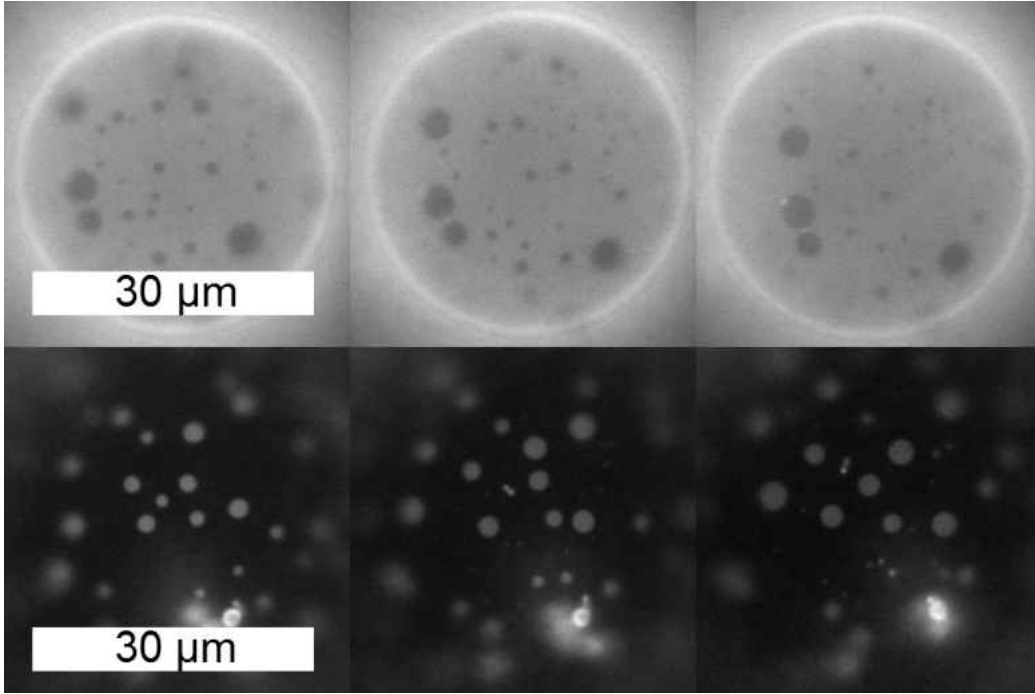


FIGURE 11. Fluorescence images from GUVs with diffusing phase separated domains. Top row: L_D majority; bottom row: L_O majority. In each case the images shown were captured 4 seconds apart.

Analysis of Tracer Motion

Given a set of single particle positions $\mathbf{x}(t_n)$ measured at times t_1, t_2, \dots, t_N , each separated by an interval Δt , (for instance from time series data such as we obtained using the process detailed above), estimating the particle's diffusion coefficient is a well-defined task, for which there exists an explicit, unbiased, and nearly optimal estimator based on the covariance of the displacements [48]. (A linear fit of the mean-squared displacements $\Delta \mathbf{x}^2(\tau)$ vs. the time interval of the displacement, τ , though often employed, does not provide a good estimate due the correlation of the values with one another; in fact, it can have the perverse property of becoming less accurate as the number of data points increases [48].) The covariance-based estimator is given by

$$D = \langle \Delta \mathbf{x}_n^2 \rangle / (2\Delta t) + \langle \Delta \mathbf{x}_n \Delta \mathbf{x}_{n+1} \rangle / \Delta t, \quad (4.4)$$

where $\Delta \mathbf{x}_n = \mathbf{x}(t_n) - \mathbf{x}(t_{n-1})$ is the displacement over one time step and the angle bracket indicates an average over all time steps. Moreover, the approach described in Ref. [48] provides

a measure of the goodness of fit (χ^2) of an observed trajectory to a purely Brownian one via comparison of its periodogram (roughly, the power spectrum of $\Delta\mathbf{x}_n$) to the functional form for free diffusion. For our lipid domains, we find the average reduced $\chi^2 = 1.25$, indicative of pure diffusion in a viscous liquid (Fig. 12).

In two-point microrheology, one considers the correlations of displacements. The radial component of the correlation tensor, D_{rr} , is determined from measurements of the displacements of tracers i and j over time τ as [85, 86]:

$$D_{rr}(R, \tau) = \langle \Delta r^i(\tau) \Delta r^j(\tau) \delta [R - R^{ij}] \rangle_{i \neq j}. \quad (4.5)$$

Here, R is the particle separation distance, R^{ij} is the distance between tracers i and j , the Δr are the components of the displacements calculated along the axis connecting the tracers' positions, and the angle brackets indicate an average over all time points and particle pairs $i \neq j$. D_{rr} increases linearly with τ for Brownian particles, much like a particle's mean square displacements. As is the case for single-point diffusion, however, this linearity is misleading and does not yield an optimal estimator for the correlation. The aim of quantifying the correlation between Brownian processes arises often in finance [92, 93], and the associated literature shows that the optimal estimator, just like in the single particle case, is formed from the covariance of single frame displacements [93].

Results

We first consider single-point viscosity measurements, determined from the dependence of the diffusion coefficients, D , of phase-separated domains on their radii, a . Our single-domain diffusion data for two of the compositions examined, a L_D majority phase (2:1 DOPC:DPPC with 20% cholesterol) and a L_O majority phase (1:2 DOPC:DPPC with 40% cholesterol), are shown in Fig. 13. Fitting to the classic two-dimensional hydrodynamic model of Hughes, Pailthorpe and White (HPW) [39], as in earlier work [34, 61], gives membrane viscosity $\eta_{1pt} = 0.75 \pm 0.15$ nPa·s·m for the L_D majority phase, and $\eta_{1pt} = 3.90 \pm 0.42$ nPa·s·m for the L_O majority phase, with uncertainties assessed by jackknife error estimation [51]. As expected, the L_O phase is more viscous than the L_D phase [61]. The HPW model applies to solid inclusions, however recent calculations of the mobility of liquid domains in fluid membranes [41, 94] indicate that for the

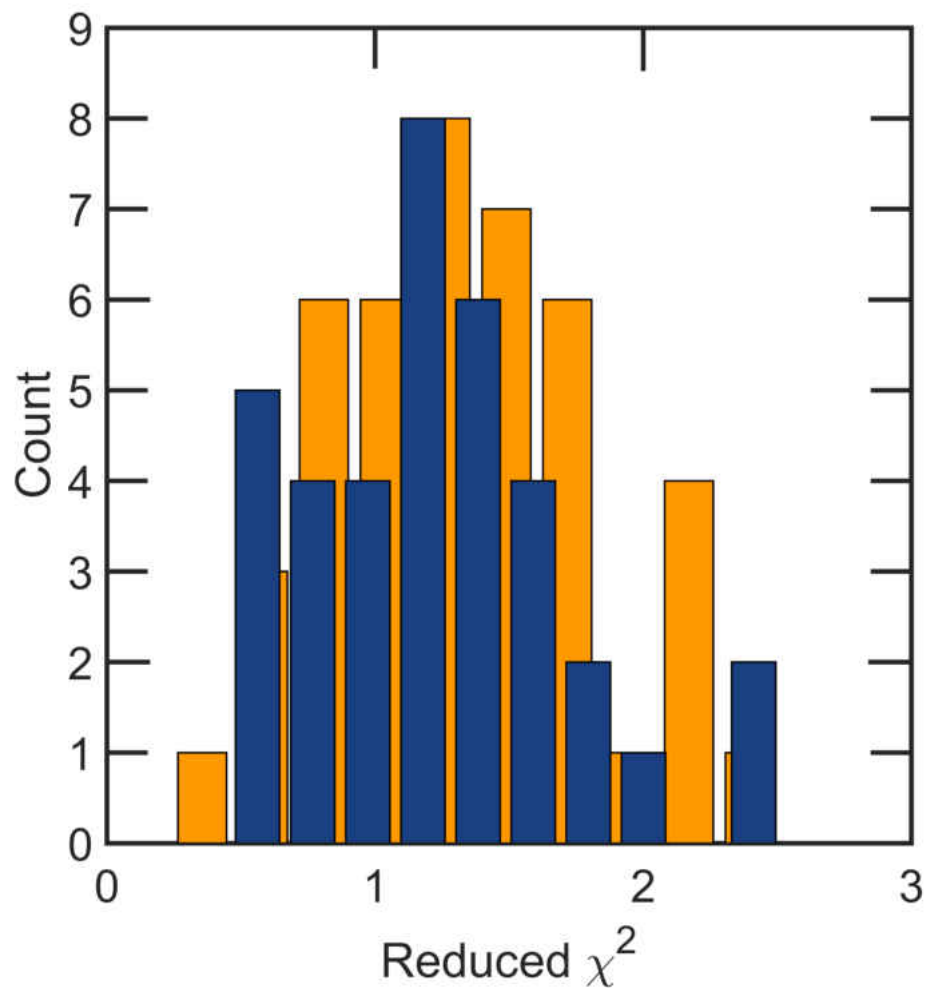


FIGURE 12. Histogram of reduced χ^2 values obtained by comparing tracer motion with the expected form for free diffusion. Binned values for the L_O majority composition 2:1 DPPC:DOPC with 40% cholesterol are shown in blue; corresponding bins for the L_D majority composition 1:2 DPPC:DOPC with 20% cholesterol are shown in orange.

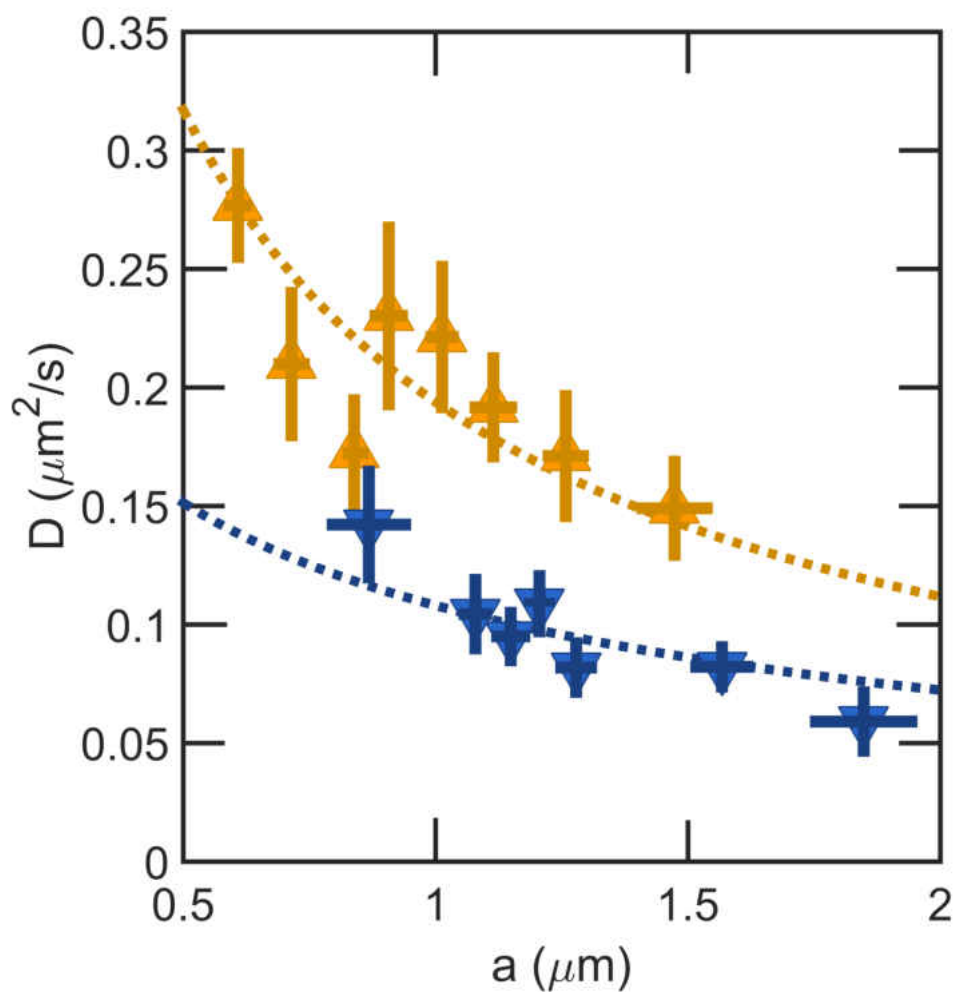


FIGURE 13. Single-point microrheology: radius dependence of domain diffusion coefficients. Shown are data from two different GUV compositions considered, a L_D majority phase (2:1 DOPC:DPPC with 20% cholesterol) in orange and a L_O majority phase (1:2 DOPC:DPPC with 40% cholesterol) in blue. Points are averages from roughly 10 domains each, with error bars indicating the standard deviation. Curves represent fits to the HPW model of $D(a)$ with bilayer viscosity as the single free parameter.

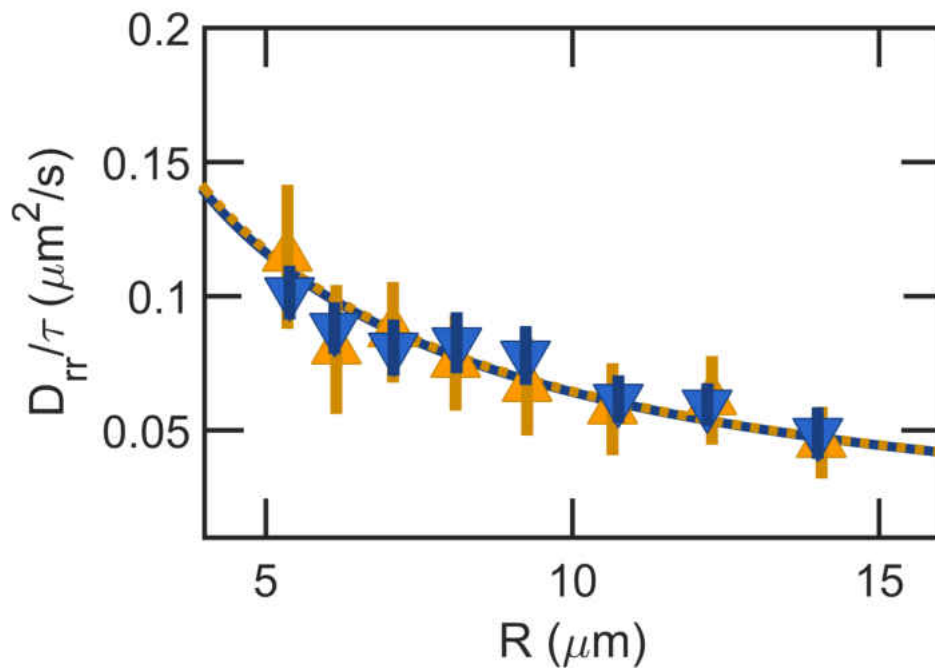


FIGURE 14. Two-point correlations D_{rr} and determination of viscosities. Shown are data from the same two GUV compositions as in Fig. 13, with L_D majority data in orange and L_O majority data in blue. Curves represent fits to Equation 3. Each point is the average of more than one hundred measurements of D_{rr} , with error bars indicating the standard deviation.

conditions observed in our experiments, corrections to the HPW model will be approximately a few percent in magnitude, well within the uncertainty of our measurements.

Similarly, we can calculate viscosity from the two-point correlations measured from the same trajectories. From Ref. [85], the expected form is

$$\frac{D_{rr}(R, \tau)}{\tau} = \frac{k_B T}{2\pi\eta} \left[\frac{\pi}{\beta} H_1(\beta) - \frac{2}{\beta^2} - \frac{\pi}{2} [Y_0(\beta) + Y_2(\beta)] \right], \quad (4.6)$$

where $\beta = 2R\eta_B/\eta$ is the reduced tracer separation, η_B is the viscosity of the aqueous medium surrounding the bilayer, H_ν are Struve functions, and Y_ν are Bessel functions of the second kind.

We find that the dependence of the measured correlations on domain separation agrees with the expected theoretical form (Fig. 14). However, in contrast to the single-point measurements, we find that the viscosities of the two compositions as measured from two-point correlations are indistinguishable within uncertainties: $\eta_{2\text{pt}} = 2.76 \pm 1.45$ nPa·s·m for the L_D majority phase, and $\eta_{2\text{pt}} = 2.95 \pm 0.61$ nPa·s·m for L_O majority phase. Furthermore, we note that these values are similar to the average of the single point results for the two majority phases: 2.32 nPa·s·m.

It appears that two-point microrheology of minority-phase lipid domains returns a value for membrane viscosity that is intermediate between those of the majority and minority phases. To test whether this is merely a peculiarity of the compositions examined for the data in Fig. 13 and 14 or a more robust feature of phase-separated vesicles, we measured one- and two-point-derived viscosities over a range of GUV compositions for which the single-point-derived majority phase viscosity spans nearly two orders of magnitude (Fig. 15). For L_O majority-phase lipids spanning 1:1 to 1:9 DOPC:DPPC, we find that the ratios of $\eta_{2\text{pt}}/\eta_{1\text{pt}}$ are less than 1, with $\eta_{2\text{pt}} = (0.77 \pm 0.05) \times$ the single-point viscosity (Fig. 15, blue symbols). Analogously, for L_D majority-phase lipids of 2:1 and 4:1 DOPC:DPPC, $\eta_{2\text{pt}}/\eta_{1\text{pt}}$ is greater than 1, with $\eta_{2\text{pt}} = (3.07 \pm 0.86) \times$ the single-point viscosity (Fig. 15, orange symbols).

Discussion

We report the first demonstration that two-point microrheology can be applied to lipid membranes, providing a sensitive test of the applicability of continuum two-dimensional hydrodynamic models to lipid systems. Despite their topographic distortions [54] and potential for long-range interactions [95], phase-separated membrane domains show a distance-dependent

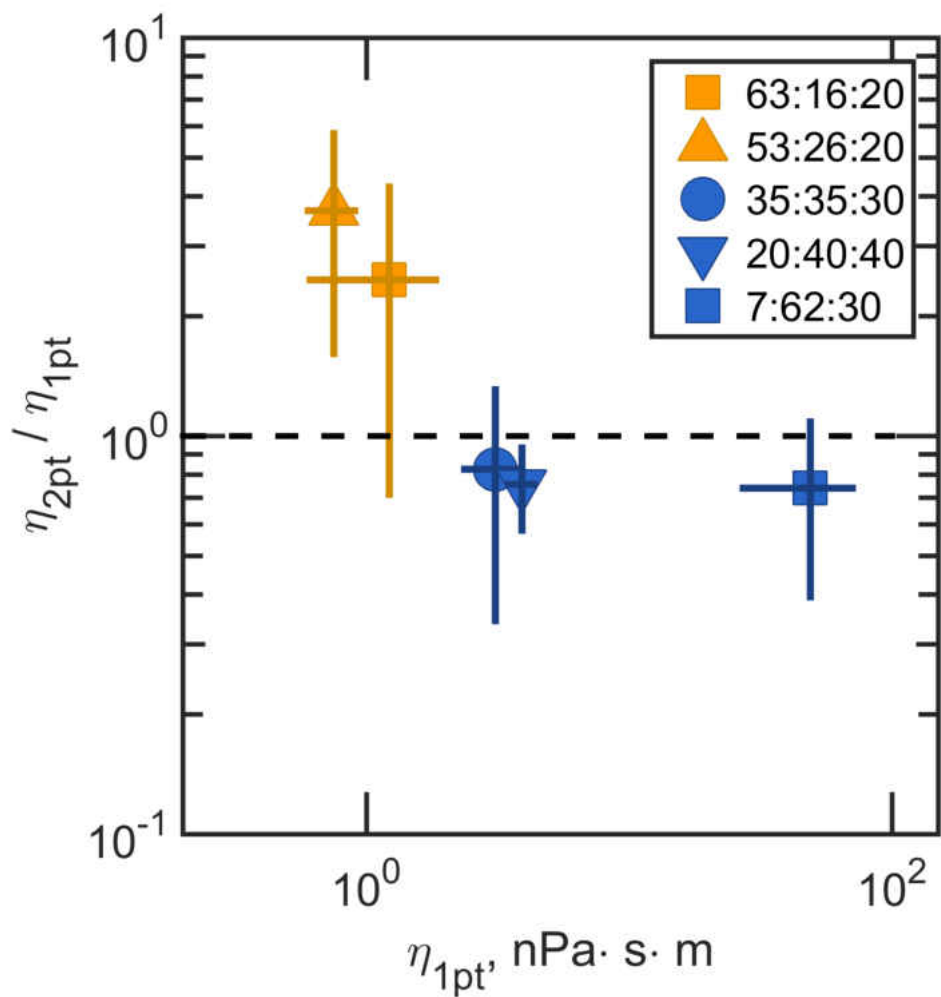


FIGURE 15. Ratio of the viscosities derived from two- and one-point methods as a function of single-point viscosity for a range of different compositions. Blue icons indicate compositions that are majority L_O , while orange symbols indicate compositions that are majority L_D . Compositions are given as mol% DOPC:DPPC:cholesterol.

correlation in their Brownian dynamics with a functional form in remarkably good agreement with theories of two-dimensional fluid response.

More importantly, our results imply that two-point measurements report an effective global membrane viscosity, amalgamating the characteristics of compositionally different regions of the membrane, while single-point measurements probe the viscosity of the majority phase surrounding tracer domains. This is perhaps to be expected for a two-dimensional fluid, since hydrodynamic correlations in two-dimensions are intrinsically long-ranged. Relatedly, recent theoretical work points to a strong sensitivity of in-plane correlations to static inclusions, even at low concentrations, again driven by long-range interactions [96]. It would be interesting to develop methods to examine, both theoretically and experimentally, two-point viscosity as a function of the area fraction of the minority phase to determine the weighting of the properties of different regions toward the overall response. We also note that existing theories of two-point correlations are formulated for small, rigid inclusions. Though their forms fit our observations, we hope that our work will spur the development of models that explicitly consider the dynamics of finite-sized fluid domains, as has recently been done for single-domain diffusion [41, 94].

We stress that, in contrast to various three-dimensional complex fluids for which two-point methods give measures of viscosity relatively uncontaminated by the distortions of local probes, our results imply that two-point methods applied to phase-separated membranes should not be considered “better” than single-point methods. Rather, the latter provide insights into the viscosity of particular phases, while the former provide insights into the larger-scale effective viscosity of a heterogeneous fluid. We note that cellular membranes exhibit a far greater degree of heterogeneity in structure and composition than the model bilayers examined here. It would be interesting to examine whether, similarly, two-point viscosity using various cellular membrane probes would show robust features that average over small-scale heterogeneity.

CHAPTER V

CONCLUSION AND OUTLOOK

The experiments and results presented in the last chapter represent the outcome of our efforts to develop new methods for measuring lipid bilayer viscosity. Together, they comprise general and complimentary techniques.

A few words on the tracers selected for our studies. In our study on GUVs, we employed phased separated domains as tracers. In many ways, these are the best possible tracer: as constituents of the bilayer themselves, they do not perturb the bilayer like beads or other tracers that must be associated with the membrane through a linkage scheme, and their extended nature make tracking and assessment of their size relatively simple. However, they are extremely limiting in the sense that they can only be employed for very specific membrane compositions. Whether such compositions are an acceptable limitation will depend on the specifics and goals of the experiment being attempted.

On the other hand, our data indicates that the use of extrinsic tracers like beads does perturb the local bilayer environment. If this effect is unaccounted for, the experiment will suffer. Our bead linkage scheme is one method for mitigating this concern, but really any asymmetric tracer will do the trick. Once such precautions have been taken, any membrane composition in which a small quantity of biotinylated lipids are included are open for exploration.

Additionally, there is nothing preventing these techniques from being combined. Future experiments that would utilize both approaches would be able to accurately measure the viscosity and characterize the heterogeneity of a bilayer composition.

We therefore have the means to examine a number of bilayer phenomena. I'll briefly discuss two experiments that we have spent some time exploring, the first being the affect of membrane tension on bilayer viscosity.

Tension is an attractive target for a biophysicist since it represents another physical parameter, like temperature, that could conceivably affect lipid bilayers. A simple experiment would involve sequentially varying the tension on a bilayer, and measuring the viscosity. The main hurdle is finding a simple means of varying membrane tension. I would claim that it is currently unknown whether such a method exists; however, one approach that is at least conceptually, if not

experimentally, simple, makes use of micropipette aspiration[97]. Here, flow in to a micropipette from the bulk reservoir can pull a GUV located at the pipette tip partially into the micropipette channel, increasing tension on the GUV. Such flows are easy to achieve by elevating the fluid reservoir containing the GUV samples above a second reservoir attached to the micropipette, thereby creating a pressure differential between the chambers that is proportional to their height:

$$\Delta P = \rho g \Delta h, \tag{5.1}$$

where ΔP is the pressure difference, ρ is the density of water, g is the gravitational constant and Δh is the height difference between the reservoirs. The tension on the membrane is then found from

$$\Delta P = 2T \left(\frac{1}{R_P} - \frac{1}{R_G} \right), \tag{5.2}$$

where T is the tension, R_G is the radius of the GUV and R_P is the radius of the micropipette.

Our preliminary results are shown in Fig. 16. The data shown is for a 20:40:40 DOPC:DPPC:Cholesterol mol percent GUV composition. We are able to increase tension over three orders of magnitude, over which we see a decrease in membrane viscosity. One possible explanation for this behavior could be that, as tension increases, domains bulge less from the GUV surface, leading to decreased drag from the bulk; this will be easy to check by imaging GUV's at various tensions near their equators. Another hypothesis is that, as tension is increased, lipids are pulled farther apart and therefore occupy a larger area within the bilayer, which is again a reasonable mechanism for reducing viscosity. Unfortunately, this later hypothesis would be difficult to verify.

Another experiment that can be attempted in the near future would involve measuring modulation of bilayer viscosity by different proteins. Our lab has some experience working with SpoVM, a protein that localizes on the surface of *Bacillus subtilis* during spore formation[98]. Experiments have shown that SpoVM is sensitive to membrane curvature[99], and therefore is able to sense material configurations of the bilayer. Using our microrheological techniques, we could assess if the protein also modulates material properties or membrane organization. Proteins like SpoVM, or Sar1, that interact with membrane curvature, are attractive targets because such

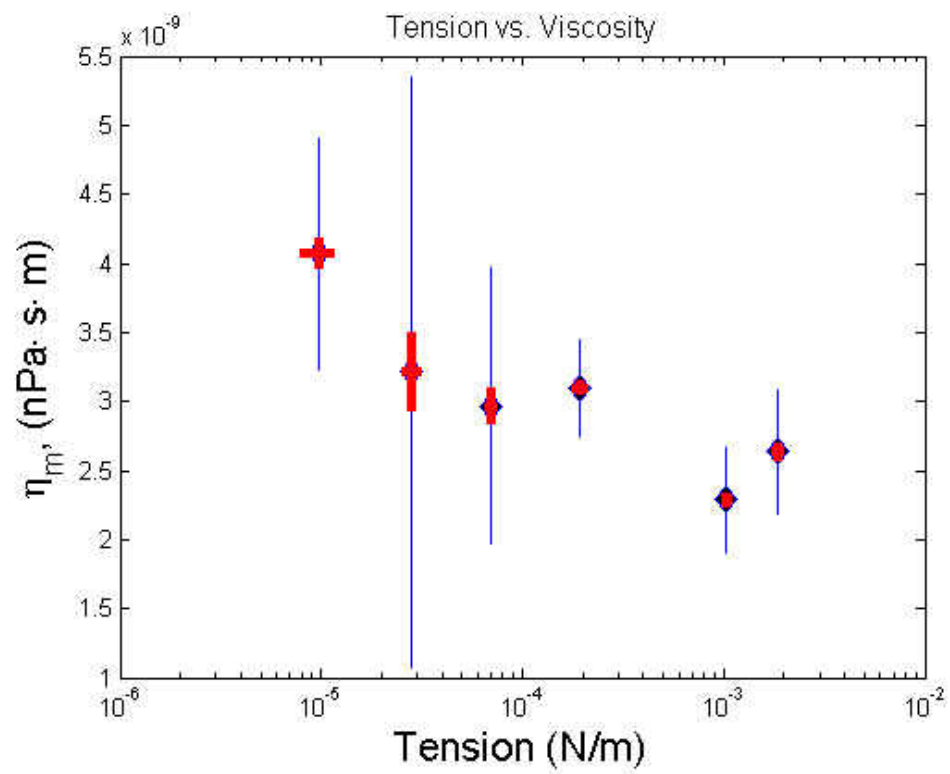


FIGURE 16. Viscosity of GUV's under different tensions calculated from one-point microrheology.

interactions indicate that they have some means of interacting directly with and are sensitive to the local bilayer environment. By examining these, and other similar proteins, we could seek to uncover mechanical similarities in function that are perhaps not obvious from protein structure.

These are just two possible directions that future work could take. But we could have similarly asked how a large cast of biological molecules or physical parameters modulate viscosity. My dissertation research developed experimental methods that will make answering such questions possible.

REFERENCES CITED

- [1] R. Lipowsky and E. Sackmann. *Structure and Dynamics of Membranes*. Elsevier, Amsterdam, The Netherlands, 1995.
- [2] Edward D. Korn. Cell membranes: structure and synthesis. *Annual Review of Biochemistry*, 38: 263 – 288, 1969.
- [3] Guido Guidotti. Membrane proteins. *Annual Review of Biochemistry*, 41:731–752, 1972.
- [4] Daniel O. Daley, Mikaela Rapp, Erik Granseth, , Karin Melèn, David Drew, and Gunnar von Heijne. Global topology analysis of the escherichia coli inner membrane proteome. *Science*, 308:1321 – 1323, 2005.
- [5] Sean Munro. Lipid rafts: Elusive or illusive? *Cell*, 115:377 – 388, 2003.
- [6] S. J. Singer and Garth Nicolson. The fluid mosaic model of the structure of cell membranes. *Science*, 175:720–31, 1972.
- [7] Gerrit van Meer, Dennis R. Voelker, and Gerald W. Feigenson. Membrane lipids: where they are and how they behave. *Nature Reviews Molecular Cell Biology*, 9:112 – 124, 2008.
- [8] Philip Yeagle. *The Structure of Biological Membranes*. CRC Press, Florida, USA, 2005.
- [9] John Katsaras and Thomas Gutberlet. *Lipid Bilayers Structures and Interactions*. Springer, Berlin, Germany, 2001.
- [10] R. Mendelsohn, M. A. Davies, J. W. Brauner, H. F. Schuster, and R. A. Dluhy. Quantitative determination of conformational disorder in the acyl chains of phospholipid bilayers by infrared spectroscopy. *Biochemistry*, 28:8934–8939, 1989.
- [11] Peter Quinn and Claude Wolf. The liquid-ordered phase in membranes. *Biochimica et Biophysica Acta - Biomembranes*, 1788:33 – 46, 2009.
- [12] Richard A. Cooper. Influence of increased membrane cholesterol on membrane fluidity and cell function in human red blood cells. *Journal of Supramolecular Structure*, 8:413 – 430, 1978.
- [13] Sloban M. Scanlon, , D. Clive Williams, and Patrick Schloss. Membrane cholesterol modulates serotonin transporter activity. *Biochemistry*, 40:10507 – 10513, 2001.
- [14] Michal Rotenberg and David Zakim. Effects of cholesterol on the function and thermotropic properties of pure udp-glucuronosyltransferase. *Journal of Biological Chemistry*, 266:4159 – 4161, 1991.
- [15] Pieter R. Cullis, Michael J. Hope, and Colin P. S. Tilcock. Lipid polymorphism and the roles of lipids in membranes. *Chemistry and Physics of Lipids*, 40:127 – 144, 1986.
- [16] Gregor Cevc. Polymorphism of the bilayer membranes in the ordered phase and the molecular origin of the lipid pretansition and rippled lamellae. *biochimica et biophysica acta*, 1062:59 – 69, 1991.
- [17] Todd P. W. McMullen, Ruthven N. A. H. Lewis, and Ronald N. McElhaney. Calorimetric and spectroscopic studies of the effects of cholesterol on the thermotropic phase behavior and organization of a homologous series of linear saturated phosphatidylglycerol bilayer membranes. *Biochimica et Biophysica Acta - Biomembranes*, 1788:345–357, 2009.

- [18] Ruthven N. A. H. Lewis, Nanette Mak, and Ronald N. McElhaney. A differential scanning calorimetric study of the thermotropic phase behavior of model membranes composed of phosphatidylcholines containing linear saturated fatty acyl chains. *Biochemistry*, 26: 6118–6126, 1987.
- [19] Jörg H. Kleinschmidt and Lukas K. Tamm. Structural transitions in short-chain lipid assemblies studied by $(31)\text{P}$ -nmr spectroscopy. *Biophysical journal*, 83:994–1003, 2002.
- [20] Hector L. Casal and Ronald N. McElhaney. Quantitative determination of hydrocarbon chain conformational order in bilayers of saturated phosphatidylcholines of various chain lengths by fourier transform infrared spectroscopy. *Biochemistry*, 29:5423–5427, 1990.
- [21] Winchil L. C. Vaz, Robert M. Clegg, and Dieter Hellman. Translational diffusion of lipids in liquid crystalline phase phosphatidylcholine multibilayers. a comparison of experiment with theory. *Biochemistry*, 24:781 – 786, 1985.
- [22] Göran Linblom and Gregor Orädd. Nmr studies of translational diffusion in lyotropic liquid crystals and lipid membranes. *Progress in NMR spectroscopy*, 26:483–515, 1994.
- [23] Zenon Derzko and Kenneth Jacobson. Comparative lateral diffusion of fluorescent lipid analogues in phospholipid multibilayers. *Biochemistry*, 19:6050 – 6057, 1980.
- [24] Manish Sud, Eoin Fahy, Dawn Cotter, Alex Brown, Edward A. Dennis, Cristopher K. Glass, Alfred H. Merrill Jr, Robert C. Murphy, Christian R. H. Raetz, David W. Russell, and Shankar Subramaniam. Lmsd: Lipid maps structure database. *Nucleic Acids Research*, 35: 527 – 532, 2007.
- [25] Todd P. W. McMullen, Ruthven N. A. H. Lewis, and Ronald N. McElhaney. Differential scanning calorimetric and fourier transform infrared spectroscopic studies of the effects of cholesterol on the thermotropic phase behavior and organization of a homologous series of linear saturated phosphatidylserine bilayer membranes. *Biophysical Journal*, 79:2056–2065, 2000.
- [26] Paulo F. F. Almeida, Winchil L. C. Vaz, and T. E. Thompson. Lateral diffusion in the liquid phases of dimyristoylphosphatidylcholine/cholesterol lipid bilayers: a free volume analysis. *Biochemistry*, 31:6739 – 6747, 1992.
- [27] Kieth W. Butler, Kenneth G. Johnson, and Ian C. P. Smith. *Acholeplasma laidlawii* membranes: an electron spin resonance study on the influence on molecular order of fatty acid composition and cholesterol. *Archives of Biochemistry and Biophysics*, 191:289 – 297, 1978.
- [28] Linda J. Pike. Rafts defined: a report on the keystone symposium on lipid rafts and cell function. *Journal of Lipid Research*, 47:1597 – 1598, 2006.
- [29] Sarah Veatch and Sarah Keller. Separation of liquid phases in giant vesicles of ternary mixtures of phospholipids and cholesterol. *Biophysical Journal*, 85:3074 – 83, 2003.
- [30] Marcus D. Collins and Sarah L. Keller. Tuning lipid mixtures to induce or suppress domain formation across leaflets of unsupported asymmetric bilayers. *Proceedings of the National Academy of Sciences of the United States of America*, 105:124 – 8, 2008.
- [31] N. Wilke and B. Maggio. The influence of domain crowding on the lateral diffusion of ceramide-enriched domains in a sphingomyelin monolayer. *The journal of physical chemistry. B*, 113:12844 – 51, 2009.

- [32] Brian A. Camley, Cinzia Esposito, Tobias Baumgart, and Frank L. H. Brown. Lipid bilayer domain fluctuations as a probe of membrane viscosity. *Biophysical Journal*, 99:L44 – 6, 2010.
- [33] Dong Chen and Maria M. Santore. Large effect of membrane tension on the fluid-solid phase transitions of two-component phosphatidylcholine vesicles. *Proceedings of the National Academy of Sciences of the United States of America*, 111:179 – 84, 2014.
- [34] Pietro Cicuta, Sarah L. Keller, and Sarah L. Veatch. Diffusion of liquid domains in lipid bilayer membranes. *The journal of physical chemistry B*, 111:3328 – 31, 2007.
- [35] Eugene P. Petrov, Rafayel Petrosyan, and Petra Schwille. Translational and rotational diffusion of micrometer-sized solid domains in lipid membranes. *Soft Matter*, 8:L41 – 3, 2012.
- [36] R. Kubo. The fluctuation-dissipation theorem. *Reports on Progress in Physics*, 29:255 – 284, 1966.
- [37] Horace Lamb. *Hydrodynamics*. Dover Publications, New York, USA, 1945.
- [38] P. G. Saffman and M. Delbrück. Brownian motion in biological membranes. *Proceedings of the National Academy of Sciences of the United States of America*, 72:3111 – 13, 1975.
- [39] B. D. Huhes, B. A. Pailthorpe, and L. R. White. The translational and rotational drag on a cylinder moving in a membrane. *Journal of Fluid Mechanics*, 110:349 – 372, 1981.
- [40] A. Naji, A. Levine, and P. Pincus. Corrections to the saffman-delbruck mobility for membrane bound proteins. *Biophysical Journal*, 93:L49–51, 2007.
- [41] Youhei Fujitani. Drag coefficient of a liquid domain in a fluid membrane. *Journal of the Physical Society of Japan*, 80:1 – 8, 2011.
- [42] Talley J. Lambert and Jennifer C. Waters. Assessing camera performance for quantitative microscopy. *Methods in Cell Biology*, 123:35 – 53, 2014.
- [43] Rafael C. Gonzalez, Richard E. Woods, and Steven L. Eddins. *Digital images processing using MATLAB*. Gatesmark, United States, 2009.
- [44] Alexander R. Small and Raghuvver Parthasarathy. Superresolution localization methods. *Annual Review of Physical Chemistry*, 65:107 – 25, 2014.
- [45] Raghuvver Parthasarathy. Rapid, accurate particle tracking by calculation of radial symmetry centers. *Nature Methods*, 9:724 – 6, 2012.
- [46] Richard W. Cole, Tushare Jinadasa, and Claire M. Brown. Measuring and interpreting point spread functions to determine confocal microscope resolution and ensure quality control. *Nature Protocols*, 6:1929 – 41, 2011.
- [47] Steven M. Kay. *Fundamentals of Statistical Signal Processing*. Prentice Hall, New Jersey, United States, 1993.
- [48] Christian L. Vestergaard, Paul C. Blainey, and Henrik Flyvberg. Optimal estimation of diffusion coefficients from single-particle trajectories. *Physical Review E*, 89:022726, 2014.
- [49] René Andrae, Tim Schulze-Hartung, and Peter Melchior. Do’s and dont’s of reduced chi squared. *arxiv*, 2010.

- [50] H. A. Sprang. A review of minimization techniques for nonlinear functions. *Society for industrial and applied mathematics review*, 4:343 – 365, 1962.
- [51] B. Efron. Nonparametric estimates of standard error: The jackknife, bootstrap and other methods. *Biometrika*, 68:589 – 599, 1981.
- [52] I. Koltover, J. O. Raedler, T. Salditt, K. J. Rothschild, and C. R. Safinya. Phase behavior and interactions of the membrane-protein bacteriorhodopsin. *Physical Review Letters*, 82:3184, 1999.
- [53] Raoul N. Frese, Josep C. Pàmies, John D. Olsen, Svetlana Bahatyrova, Chantal D. van der Weij-de Wit, Thijs J. Aartsma, Cees Otto, C. Neil Hunter, Daan Frenkel, and Rienk van Grondelle. Protein shape and crowding drive domain formation and curvature in biological membranes. *Biophysical Journal*, 94:640 – 647, 2008.
- [54] T. Baumgart, S. T. Hess, and W. W. Webb. Imaging coexisting fluid domains in biomembrane models coupling curvature and line tension. *Nature*, 824:821 – 824, 2003.
- [55] T. G. Mason and D. A. Weitz. optical measurements of frequency-dependent linear viscoelastic moduli of complex fluids. *Physical Review Letters*, 74:1250 – 1253, 1995.
- [56] T. Mason, K. Ganesan, J. van Zanten, D. Wirtz, and S. Kuo. Particle tracking microrheology of complex fluids. *Physical Review Letters*, 79:3282–3285, 1997.
- [57] B. D. Hoffman and J. C. Crocker. Multiple-particle tracking and two-point microrheology in cells. *Methods in Cell Biology*, 83:141 – 178, 2007.
- [58] Derek Marsh. *Handbook of Lipid Bilayers*. CRC Press, Boca Raton, FL, 2013.
- [59] R. Machañ and M. Hof. Lipid lateral diffusion in planar bilayers investigated by fluorescence correlation spectroscopy. *Biochimica et Biophysica Acta*, 1798:1377 – 1391, 2010.
- [60] G. Barnes and I. Gentle. *Interfacial Science: An Introduction*. Oxford University Press, Oxford UK, 1995.
- [61] C. Stanich, A. Honerkamp-Smith, G. Putzel, C. Warth, A. Lamprecht, P. Mandal, E. Mann, T. Hua, and S. Keller. Coarsening dynamics of domains in lipid membranes. *Biophysical Journal*, 105:444 – 454, 2013.
- [62] M. Sickert, F. Rondelez, and H. Stone. Single-particle brownian dynamics for characterizing the rheology of fluid langmuir monolayers. *Europhysics Letters*, 79:66005, 2007.
- [63] John R. Silvius. *Thermotropic Phase Transitions of Pure Lipids in Model Membranes and Their Modifications by Membrane Proteins*. John Wiley & Sons, New York, NY, 1982.
- [64] Cristopher W. Harland, David Rabuka, Carolyn R. Bertozzi, and Raghuvver Parthasarathy. The m. tuberculosis virulence factor trehalose dimycolate imparts desiccation resistance to model mycobacterial membranes. *Biophysical Journal*, 94:4718 – 4724, 2008.
- [65] A. Honerkamp-Smith, B. Machta, and S. Keller. Experimental observations of dynamic critical phenomena in lipid membranes. *Physical Review Letters*, 108:265702, 2012.
- [66] R. Dimova, C. Dietrich, A. Hadjiisky, K. Danov, and B. Pouligny. Falling ball viscosimetry of giant vesicle membranes: finite-size effects. *European Physical Journal B*, 12:589 – 598, 1999.
- [67] C. Herold, P. Schwille, and E. P. Petrov. Dna condensation at freestanding cationic lipid bilayers. *Physical Review Letters*, 104:148102, 2010.

- [68] H. McMahon and J. Gallop. Membrane curvature and mechanisms of dynamic cell membrane remodelling. *Nature*, 438:590 – 596, 2005.
- [69] J. Zimmerberg and M. Kozlov. How proteins produce cellular membrane curvature. *Nature Reviews Molecular Cell Biology*, 7:9 – 19, 2006.
- [70] R. Parthasarathy and J. Groves. Curvature and spatial organization in biological membranes. *Soft Matter*, 3:24, 2007.
- [71] A. Nakaño and M. Muramatsu. A novel gtp-binding protein, sar1p, is involved in transport from the endoplasmic reticulum to the golgi apparatus. *The Journal of Cell Biology*, 109:2677 – 2691, 1989.
- [72] C. Barlowe, C. D’enfert, and R. Schekman. Purification and characterization of sar1p, a small gtp-binding protein required for transport vesicle formation from the endoplasmic reticulum. *The Journal of Biological Chemistry*, 268:873 – 879, 1993.
- [73] M. Lee, L. Orci, S. Hamamoto, E. Futai, M. Ravazzola, and R. Schekman. Sar1p n-terminal helix initiates membrane curvature and completes the fission of a copii vesicle. *Cell*, 122:605 – 617, 2005.
- [74] E. Settles, A. Loftus, A. McKeown, and R. Parthasarathy. The vesicle trafficking protein sar1 lowers lipid membrane rigidity. *Biophysical Journal*, 99:1539 – 1545, 2010.
- [75] A. Loftus, S. Noreng, V. Hsieh, and R. Parthasarathy. Robust measurement of membrane bending moduli using light sheet fluorescence imaging of vesicle fluctuations. *Langmuir*, 29:14588 – 14594, 2013.
- [76] K. Matsuoka, L. Orci, M. Amherdt, S. Bednarek, and S. Hamamoto. Copii-coated vesicle formation reconstituted with purified coat proteins and chemically defined liposomes. *Cell*, 93:263 – 275, 1998.
- [77] A. F. Loftus, V. Hsieh, and R. Parthasarathy. Modulation of membrane rigidity by the human vesicle trafficking proteins sar1a and sar1b. *Biochemical and Biophysical Research Communications*, 426:585 – 589, 2012.
- [78] T. Hormel, S. Kurihara, M. Brennan, M. Wozniak, and R. Parthasarathy. Measuring lipid membrane viscosity using rotational and translational probe diffusion. *Physical Review Letters*, 112:188101, 2014.
- [79] J. Crocker, M. Valentine, E. Weeks, T. Gisler, P. Kaplan, A. Yodh, and D. Weitz. Two-point microrheology of inhomogeneous soft materials. *Physical Review Letters*, 85:888 – 891, 2000.
- [80] A. Lau, B. Hoffman, A. Davies, J. Crocker, and T. Lubensky. Microrheology, stress fluctuations, and active behavior of living cells. *Physical Review Letters*, 91:198101, 2003.
- [81] J. Liu, M. Gardel, K. Kroy, E. Frey, B. Hoffman, J. Crocker, A. Bausch, and D. Weitz. Microrheology probes length scale dependent rheology. *Physical Review Letters*, 96:118104, 2006.
- [82] J. Crocker and B. Hoffman. Multiple-particle tracking and two-point microrheology in cells. *Methods in Cell Biology*, 83:141 – 78, 2007.
- [83] M. Garel, M. Valentine, J. Crocker, A. Bausch, and D. Weitz. Microrheology of entangled f-actin solutions. *Physical Review Letters*, 91:158302, 2003.
- [84] L. Starrs and P. Bartlett. One- and two-point micro-rheology of viscoelastic media. *Journal of Physics: Condensed Matter*, 15:S251, 2003.

- [85] A. Levine and F. MacKintosh. Dynamics of viscoelastic membranes. *Physical Review E*, 66:061606, 2002.
- [86] V. Prasad, S. Koehler, and Eric Weeks. Two-particle microrheology of quasi-2d viscous systems. *Physical Review Letters*, 97:176001, 2006.
- [87] V. Prasad and E. Weeks. Two-dimensional to three-dimensional transition in soap films demonstrated by microrheology. *Physical Review Letters*, 102:178302, 2009.
- [88] V. Prasad and E. Weeks. Flow fields in soap films: Relating viscosity and film thickness. *Physical Review E*, 80:026309, 2009.
- [89] Sarah L. Veatch and Sarah L. Keller. Miscibility phase diagrams of giant vesicles containing sphingomyelin. *Physical Review Letters*, 148101:3 – 6, 2005.
- [90] S. Veatch. Electroformation and fluorescence microscopy of giant vesicles with coexisting liquid phases. *Methods in Molecular Biology*, 389:59 – 72, 2007.
- [91] C. Tomasi and R. Manduchi. Bilateral filtering for gray and color images, 1998.
- [92] K. Düllmann, J. Küll, and M. Kunisch. Estimating asset correlations from stock prices or default rates - which method is superior? *J. Econ. Dyn. Control.*, 34:2341 – 2357, 2008.
- [93] R. Jones. Estimating correlated diffusions, 1999. URL <http://www.sfu.ca/~rjones/econ811/readings/correl.pdf>.
- [94] Youhei Fujitani. Drag coefficient of a liquid domain in a fluid membrane surrounded by confined three-dimensional fluids. *Journal of the Physical Society of Japan*, 82:1 –12, 2013.
- [95] S. Rozovsky, Y. Kaizuka, and J. Groves. Formation and spatio-temporal evolution of periodic structures in lipid bilayers. *Journal of the American Chemical Society*, 127:36 – 37, 2005.
- [96] Naomi Oppenheimer and Haim Diamant. In-plane dynamics of membranes with immobile inclusions. *Physical Review Letters*, 107:258102, December 2011.
- [97] Robert M. Hochmuth. Micropipette aspiration of living cells. *Journal of Biomechanics*, 33:15 – 22, 2000.
- [98] Simon Cutting, Michelle Anderson, Elena Lysenko, Anthony Page, Toshifumi Tomoyasu, Kenji Tatematsu, Takashi Tatsuta, Lee Kroos, and Teru Ogura. Spovm, a small protein essential to development in bacillus subtilis, interacts with the atp-dependent protease ftsh. *Journal of Bacteriology*, 179:5534 – 5542, 1997.
- [99] Kumaran S. Ramamurthi, Sigolene Lecuyer, Howard A. Stone, and Richard Losick. Geometric cue for protein localization in a bacterium. *Science*, 323:1354 – 1357, 2009.